Properties of photosystem II lacking the PsbJ subunit

Alain Boussac, Julien Sellés, Marion Hamon, Miwa Sugiura

Properties of Photosystem II lacking the PsbJ subunit.

Alain Boussac[1], Julien Sellés[2], Marion Hamon[3], Miwa Sugiura[4]

[1] I[2]BC, UMR CNRS 9198, CEA Saclay, 91191 Gif-sur-Yvette, France.

[2] Institut de Biologie Physico-Chimique, UMR CNRS 7141 and Sorbonne Université, 13 rue Pierre et Marie Curie, 75005 Paris, France.

[3] Institut de Biologie Physico-Chimique, UMR8226/FRC550 CNRS and Sorbonne-Université, 13 rue Pierre et Marie Curie, 75005 Paris, France.

[4] Proteo-Science Research Center, and Department of Chemistry, Graduate School of Science and Technology, Ehime University, Bunkyo-cho, Matsuyama, Ehime 790-8577, Japan.

*Corresponding authors: alain.boussac@cea.fr, miwa.sugiura@ehime-u.ac.jp

The authors declare that they have no conflict of interest.

ORCID numbers:

Alain Boussac, 0000-0002-3441-3861

Julien Sellés, 0000-0001-9262-8257

Keywords: Photosystem II, PsbJ, plastoquinone, assembly, photoinhibition.

Acknowledgments

This work has been in part supported by i) the French Infrastructure for Integrated Structural Biology (FRISBI) ANR-10-INBS-05, ii) the Labex Dynamo (ANR-11-LABX-0011-01), iii) EQUIPEX (CACSICE ANR-11-EQPX-0008), notably through funding of the Proteomic Platform of IBPC (PPI). MS was supported by the JSPS-KAKENHI grant in Scientific Research on Innovative Areas JP17H06435 and a JSPS-KAKENHI grant 21H02447.

Abbreviations:

Chl, chlorophyll; Chl_{D1}/Chl_{D2}, accessory Chl's on the D1 or D2 side, respectively; DCMU, 3-(3,4-dichlorophenyl)-1,1-dimethylurea; PSII, Photosystem II; MES, 2–(*N*–morpholino) ethanesulfonic acid; P_{680}, primary electron donor; P_{D1} and P_{D2}; Chl monomer of P_{680} on the D1 or D2 side, respectively, Phe_{D1} and Phe_{D2}, pheophytin on the D1 or D2 side, respectively; Q_A, primary quinone acceptor; Q_B, secondary quinone acceptor; Tyr_D, redox active tyrosine 160 of D2; Tyr_Z, redox active tyrosine 161 of D1; TL, thermoluminescence; WT*3, *T. elongatus* mutant strain containing only the *psbA*$_3$ gene and a His_6-tag on the C-terminus of CP43. EPR, Electron Paramagnetic Resonance spectroscopy; MALDI-TOF, Matrix Assisted Laser Desorption Ionization - Time of Flight.

Abstract

Photosystem II (PSII), the oxygen-evolving enzyme, consists of 17 trans-membrane and 3 extrinsic membrane proteins. Other subunits bind to PSII during assembly, like Psb27, Psb28, Tsl0063. The presence of Psb27 has been proposed (Zabret et al. 2021 Nature Plants 7: 524–538; Huang et al. 2021 Proc Natl Acad Sci USA 118: e2018053118; Xiao et al. 2021 7: 1132–1142) to prevent the binding of PsbJ, a single transmembrane α-helix close to the quinone Q_B binding site. Consequently, a PSII rid of Psb27, Psb28 and Tsl0034 prior to the binding of PsbJ would logically correspond to an assembly intermediate. The present work describes experiments aiming at further characterizing such a ΔPsbJ-PSII, purified from the thermophilic *Thermosynechococcus elongatus*, by means of MALDI-TOF spectroscopy, Thermoluminescence, EPR spectroscopy and UV-visible time-resolved spectroscopy. In the purified ΔPsbJ-PSII, an active Mn_4CaO_5 cluster is present in 60-70 % of the centers. In these centers, although the forward electron transfer seems not affected, the *Em* of the Q_B/Q_B^- couple increases by ≥ 120 mV thus disfavoring the electron coming back on Q_A. The increase of the energy gap between Q_A/Q_A^- and Q_B/Q_B^- could contribute in a protection against the charge recombination between the donor side and Q_B^-, identified at the origin of photoinhibition under low light (Keren et al. 1997 Proc Natl Acad Sci USA 94: 1579–1584), and possibly during the slow photoactivation process.

Introduction

Photosystem II (PSII), the water-splitting enzyme in cyanobacteria, algae and higher plants, is responsible for the production of the atmospheric O_2 that is essential for aerobic organisms and it is the first step in the production of food, fibers and fossil fuels. The mature Photosystem II, in cyanobacteria, consists of 20 subunits (Umena et al. 2011; Suga et al. 2015) with 17 trans-membrane and 3 extrinsic membrane proteins (Roose et al. 2016). The PSII also binds 35 chlorophylls, 2 pheophytins, 2 hemes, 1 non-heme iron, 2 plastoquinones (Q_A and Q_B), the Mn_4CaO_5 cluster, 2 Cl^-, 12 carotenoids and 25 lipids (Umena et al. 2011; Suga et al. 2015). Most of the cofactors involved in the water oxidation and electron transfer bind to the reaction center subunits, PsbA (also called D1) and PsbD (also called D2).

After the absorption of a photon by one of the antenna chlorophylls, the excitation is transferred from chlorophyll to chlorophyll to the photochemical trap formed by the four chlorophylls P_{D1}, P_{D2}, Chl_{D1} and Chl_{D2}. A few picoseconds later, a charge separation occurs forming the $Chl_{D1}^+Phe_{D1}^-$ and then the $P_{D1}^+Phe_{D1}^-$ radical pairs (Holzwarth et al. 2006; Romero et al. 2017). In the ns time range, P_{D1}^+ oxidizes Tyr_Z, the Tyr161 of the D1 polypeptide. In the µs to ms time range, the radical $Tyr_Z^\bullet$ oxidizes the Mn_4CaO_5 cluster, see (Shen 2015, Cox et al. 2020) for reviews. On the electron acceptor side, Phe_{D1}^- reduces the primary quinone electron acceptor Q_A. The electron on Q_A^- is in turn transferred to the second quinone electron acceptor Q_B. Whereas Q_A is only singly reduced under normal conditions, Q_B can be doubly reduced and can bind two protons before to leave its binding site, reviewed in (de Causmaecker et al. 2019). The Mn_4CaO_5 complex is oxidised sequentially in four successive charge separations. In doing so, it passes through five redox states denoted by Sn, where n represents the number of stored oxidative equivalents (Kok et al. 1970; Joliot and Kok 1975). When the S_4-state is formed, *i.e.* after the 3rd flash of light given on dark-adapted PSII that is in the S_1-state, the two water molecules bound to the cluster are oxidized, the O_2 is released and the S_0-state is reformed.In cyanobacteria, in addition to the subunits involved in the cofactors binding (PsbA, PsbD, CP43, CP47, PsbE, PsbF), there are several small subunits consisting in only a transmembrane α-helix as PsbT, PsbM, PsbJ, PsbK, PsbL, PsbI, PsbX, PsbY, Psb30 (formerly Ycf12), *e.g.*(Kashino et al. 2002, 2007; Nowaczyk et al. 2012; Sugiura et al. 2012). Some roles have been attributed to these low molecular weight subunits either upon site directed mutagenesis, mainly for PsbT, or upon the deletion of the protein as for PsbM, PsbJ, Psb30, PsbK, PsbX, PsbZ.

It has been proposed that the interaction between Phe239 of PsbA and the PsbT subunit is required to restrict the movement of the DE loop of PsbA. In turn, the disruption of this interaction may perturb the binding of bicarbonate to the non-heme iron that could contribute to the signal for PSII to undergo a repair following photodamages (Forsman and Eaton-Rye 2021). Deletion of PsbM has been reported to mainly affect the Q_B environment (Uto et al. 2017). PSII depleted of Psb30 exhibited a lower efficiency under high light conditions and Psb30 favors the stabilization of the PSII complex (Sugiura et al. 2010a; Inoue-Kashino et al. 2011). Deletion of PsbK has been proposed to destabilize the association of PsbZ and Psb30 (Ycf12) with PSII complex and to alter the Q_B function (Iwai et al. 2010). PsbZ has been proposed to stabilize the binding of Psb30 (Takasaka et al. 2010). Deletion of PsbX has been shown to affect the PSII integrity in both *Arabidopsis thaliana* (Garcia-Cerdan et al. 2009) and *Synechocystis sp.* PCC 6803 (Funk 2000). In plant PSII, the PsbL subunit seems to prevent the back electron flow from the reduced plastoquinol pool thus protecting the PSII from photoinactivation (Ohad et al. 2004). In *Synechocystis sp.* PCC 6803, PsbL also influences forward electron transfer from Q_A^- to Q_B (Luo et al. 2014).

The *psbJ* gene belongs to the *psbEFLJ* operon coding for the PsbE and PsbF subunits bearing the two histidine residues His23 and His24, respectively, which are the heme iron axial ligands of the Cytb_{559} (Umena et al. 2011). The PsbJ subunit is close to PsbK and its possible involvement in the exchange of the plastoquinone has been discussed (Kaminskaya et al. 2007; Müh et al. 2012; van Eerden et al. 2017) with a role in the efficiency of forward electron flow following the charge separation process by affecting the Q_A and Q_B properties (Ohad et al. 2004; Regel et al. 2001). In *Synechocystis sp.* PCC 6803, double mutants lacking PsbJ and either PsbV or PsbO are unable to grow photoautotrophically (Choo et al. 2021).

In most of the deletion mutants, the observed phenotype is an alteration of the acceptor side. However, it is difficult to attribute these changes more to a specific role of the deleted subunits, rather than to perturbations in the overall structure of PSII. Cyanobacteria have several PsbA isoforms (Mulo et al. 2009; Sugiura and Boussac, 2014; Sheridan et al. 2020). In *Thermosynechococcus elongatus*, the deletion of the *psbJ* gene has different consequences with either PsbA1 or PsbA3 as the D1 protein. In PsbA3-PSII, the effects are minor whereas in the purified ΔPsbJ-PsbA1/PSII several other subunits including PsbY, PsbU, and PsbV are lacking (Sugiura et al. 2010b). In contrast, Psb27, Psb28 and Tsl0063, have been found to be associated to a proportion of the ΔPsbJ-PsbA1/PSII (Nowaczyk et al. 2012). These three proteins are known to be PSII assembly factors (Nowaczyk et al. 2006; Roose and Pakrasi 2008; Komenda et al. 2012; Liu et al. 2013; Huang et al. 2021; Zabret et al. 2021). It should

be noted that Tsl0063 is named either Psb34 in (Zabret et al. 2021) or Psb36 in (Xiao et al. 2021). Structures of PSII corresponding to assembly intermediates have been recently solved by using cryo-EM by using different strategies (Zabret et al. 2021; Huang et al. 2021; Xiao et al. 2021). Upon deletion of the *psbJ* gene it became possible to isolate a "PSII-I" intermediate with Psb27, Psb28 and Tsl0063 bound and in which the major conformational change was a distortion of the Q_B binding site and the replacement of bicarbonate with glutamate as a ligand of the non-heme iron (Zabret et al. 2021). From a *psbV* deletion mutant a dimeric Psb27-PSII (Huang et al. 2021) and Psb28-PSII (Xiao et al. 201) have also been purified in which the dissociation of PsbJ occurs. Such changes are proposed to protect the PSII from damage during biogenesis until an active Mn_4CaO_5 cluster is assembled (Zabret et al. 2021; Xial et al. 2021).

Since the presence of Psb27 prevents the binding of PsbU and induces the dissociation of PsbJ and PsbY (Huang et al. 2021) and since PsbJ also seems to trigger the release of Psb28 (Zabret et al. 2021), the binding of PsbJ during the PSII assembly process very likely occurs *after* the release of Psb27 and Psb28. Consequently, a PSII without Psb27, Psb28, Tsl0063, and without PsbJ would logically also correspond to an assembly intermediate. In the present work, we describe the results of experiments aiming at further characterizing the ΔPsbJ-PsbA1/PSII purified from *Thermosynechococcus elongatus* by means of MALDI-TOF spectroscopy, Thermoluminescence, EPR spectroscopy and UV-visible time-resolved spectroscopy.

Materials and Methods

Samples used

The *Thermosynechococcus elongatus* strains used were; *i*) the *ΔpsbA₂*, *ΔpsbA₃* deletion mutant, referred to as either WT*1-PSII or PsbA1-PSII, *ii*) the *ΔpsbA₁*, *ΔpsbA₂* deletion mutant, referred to as either WT*3-PSII or PsbA3-PSII (Sugiura et al. 2010b), and *iii*) the ΔPsbJ-43H deletion mutant (Sugiura et al. 2010b) which has the three *psbA* genes but in which only the PsbA1-PSII is produced under the culture conditions used in this work, see thereafter. These strains were constructed from the *T. elongatus* 43-H strain that had a His_6-tag on the carboxy terminus of CP43 (Sugiura and Inoue 1999). PSII purification was achieved as previously described (Sugiura et al. 2014). The final resuspending medium

contained 1 M betaine, 15 mM $CaCl_2$, 15 mM $MgCl_2$, 40 mM Mes, pH 6.5 adjusted with NaOH.

MALDI-TOF measurements

All reagents and solvents were purchased from Sigma-Aldrich (Saint Quentin-Fallavier, France) with the highest purity available. Peptides and protein used for calibration were purchased from LaserBio Labs (TOF Mix) and Sigma (equine apomyoglobin), respectively. For intact mass analysis, 1 µL of PSII complex prepared at a concentration of ~100 µg Chl /mL in the medium mentioned above was mixed with 2 µL of a saturated solution of sinapinic acid in 60/0.1 acetonitrile/trifluoroacetic acid. Two microliters of this premix were spotted onto the sample plate and allowed to dry under a gentle air stream. Spectra were acquired in positive reflectron and linear mode on an Axima Performance MALDI-TOF/TOF mass spectrometer (Shimadzu, Manchester, UK) with a pulse extraction fixed at 4000 for 3000-10000 m/z range and at 10000 for 6000-20000 m/z range acquisitions. All spectra were externally calibrated using a homemade calibrant mixture prepared by mixing 1 µL of 50 µM apomyoglobine in water with 2 µL of TOF Mix solution containing ACTH [7-38] peptide at a concentration of 6 µM.

UV-visible time-resolved absorption change spectroscopy

Absorption changes measurements have been performed with a lab-built spectro-photometer (Béal et al. 1999) slightly modified as previously described (Sugiura et al. 2020)

The samples were diluted in 1 M betaine, 15 mM $CaCl_2$, 15 mM $MgCl_2$, and 40 mM Mes (pH 6.5). PSII samples were dark-adapted for ~ 1 h at room temperature (20–22°C) before, when indicated, the addition of 0.1 mM phenyl *p*–benzoquinone (PPBQ) dissolved in dimethyl sulfoxide. The chlorophyll concentration of all the samples was ~ 25 µg of Chl/mL. After the ΔI/I measurements, the absorption of each diluted batch of samples was precisely controlled to avoid errors due to the dilution of concentrated samples and the ΔI/I values were normalized to A_{673} = 1.75, with ε ~ 70 $mM^{-1} \cdot cm^{-1}$ at 674 nm for dimeric PSII (Müh and Zouni 2005).

EPR spectroscopy

X-band cw-EPR spectra were recorded with a Bruker Elexsys 500 spectrometer previously described (Sugiura et al. 2020Flash illumination at room temperature was provided

by a neodymium:yttrium–aluminum garnet (Nd:YAG) laser (532 nm, 550 mJ, 8 ns Spectra Physics GCR-230-10). Illumination at 198 K with visible light was done in a non-silvered Dewar filled with ethanol cooled with dry ice for approximately 5-10 seconds with a 800 W tungsten lamp filtered by water and infrared cut-off filters. Illumination at 4.2 K was done in the EPR cavity using a low-voltage halogen lamp (24V, 250W, Philips Type 13163) filtered by water and infrared cut-off filters. After a 1 h dark-adaptation at room temperature the samples were frozen in the dark to 198 K in a dry ice ethanol bath and then transferred to 77 K in liquid N_2. Prior to the recording of the spectra the samples were degassed at 198 K.

Thermoluminescence measurements

Thermoluminescence (TL) curves were measured with a lab–built apparatus (Ducruet 2003; Ducruet and Vass 2009). PSII samples were diluted in 1 M betaine, 40 mM MES, 15 mM $MgCl_2$, 15 mM $CaCl_2$, pH 6.5 and then dark-adapted for at least 1 h at room temperature. When used, DCMU (100 µM, final concentration), dissolved in ethanol, was added after the dark-adaptation. Flash illumination was given at -10°C by using a saturating xenon flash. Two reasons justifies the choice of this temperature. Firstly, with the resuspending medium used, the freezing/melting of the samples occurs at ~ -15°C. Since the frozen samples are strongly diffusing, the flash illumination was done at a temperature slightly above -15°C. Secondly, an artefact occurs in the melting region which makes difficult the detection of small signals. It has been checked after the dilutions that the PSII samples had the same OD at 673 nm equal to 0.70 *i.e.* ~ 10 µg Chl/mL.

The measurements have been done on two different ΔPsbJ-PSII preparations with at least two measurements on each PSII samples except for the period 4 oscillation experiment at 291 nm done on only one PSII preparation. In addition to MALDI-TOF analysis, the protein content of the ΔPsbJ-PSII has been previously monitored with SDS-page and the oligomeric state of PSII was also analyzed by gel permeation (Sugiura et al. 2010b). Most of the ΔPsbJ-PSII, although not all, was in monomeric form and there was no evidence for the presence of any of the 3 proteins Psb28, Psb27 and Tsl0063 in significant amounts. For the spectroscopic measurements all samples were dark-adapted for one hour at room temperature before the measurements for allowing a full decay of S_2 and S_3 into S_1 (Sugiura et al. 2004).

Results

Before studying the effects of the PsbJ deletion some control experiments were performed. Indeed, it has been reported (Nowaczyk et al. 2012) that in *T. elongatus* cells having all the *psbA1*, *psbA2* and *psbA3* genes, and the *psbJ* gene inactivated by insertion of a cassette, PsbA1 was replaced by PsbA3 in the ΔPsbJ-PSII. Although this substitution was not observed in the most recent work done by the same group (Zabret et al. 2021) it seemed important to us to verify that the D1 subunit was indeed PsbA1 in our ΔPsbJ-43H/PSII which also contains the 3 genes, *psbA1*, *psbA2* and *psbA3*. For that, we have recorded the electrochromic blue shift undergone by Phe_{D1} in the Q_X spectral region upon the formation of Q_A^-. This electrochromic C-550 band shift is well known to be red shifted by ~ 3.0 nm from 544 nm in PsbA1-PSII to 547 nm in PsbA3-PSII. This shift reflects a hydrogen bond from the 13^1-keto C=O group of Phe_{D1} stronger with the carboxylate group of E130 in PsbA3-PSII than with the amine group of Q130 in PsbA1-PSII (Merry et al. 1998; Cuni et al. 2004; Hughes et al. 2010; Shibuya et al. 2010).

Figure 1 shows the C–550 bandshift with PsbA1-PSII (black spectrum), in PsbA3-PSII (blue spectrum) and in ΔPsbJ-43H/PSII (red spectrum). For these measurements, the samples were first dark–adapted for one hour at room temperature. Then, the absorption changes were measured 15 µs after each actinic flash in a series in the presence of PPBQ. The data points are the average of the individual absorption changes induced by the 2^{nd} to 7^{th} flashes. In the ΔPsbJ-43H/PSII the electrochromic band shift was similar to that in the PsbA1/PSII sample, showing unambiguously that the D1 protein is PsbA1 in the ΔPsbJ-43H/PSII.

Secondly, the polypeptide content was analysed in WT*1-PSII and ΔPsbJ-43H/PSII with MALDI-TOF spectroscopy. Panel A in Figure 2 shows the *m/z* region from 3500 to 6500. The inset in Panel A shows the *m/z* region corresponding to PsbM (4009 Da calc.) and PsbJ (4002 Da calc.) by a using the reflection mode. The different peaks for one protein correspond to the different proportions of ^{13}C in the proteins starting from no ^{13}C (100% ^{12}C) to 1, 2, 3, and so on, ^{13}C per protein. The two peaks for PsbJ spaced by ~16 *m/z* likely correspond to an oxygen adduct for the larger *m/z* value, also seen in earlier reports as in (Sugiura et al. 2010b; Nowaczyk et al. 2012). Panel B in Figure 2 shows the *m/z* region from 6500 to 16000. The PsbJ subunit, as expected, is missing in the ΔPsbJ-43H/PSII (Sugiura et al. 2010b; Nowaczyk et al. 2012). In ΔPsbJ-43H/PSII, other subunits are missing as PsbY, PsbU, PsbV (the $Cyt c_{550}$) as previously observed. However, PsbM and PsbF are now detected in 43H/ΔPsbJ-PSII exhibiting a peak with an amplitude comparable to that in WT*1-PSII and with a single peak for PsbM while two peaks (native and formylated) were previously

observed in (Sugiura et al. 2010b). The reasons for such a difference between the two observations is at present unclear. A reexamination of the raw data in (Sugiura et al. 2010b) indicates that at that time we did not pay attention to the possible presence of Psb28 in a very small proportion of our ΔPsbJ-43H/PSII. Indeed, a very small peak at *m/z* ~ 12787 was present (Sugiura et al. 2010b). Panel B in Figure 2 also shows a very small peak at 12787 that could well correspond to Psb28. However, the amplitude of this peak is close to the limit of the detection. A small peak detected at *m/z*=13424 in some traces could correspond to Psb27 (not shown). A peak at *m/z*=5936, not attributed in (Sugiura et al. 2010b) could originate from Tsl0063 recently detected in ΔPsbJ-PsbA1/PSII (Zabret et al. 2021). This protein is however not detected in Figure 2. The MALDI-TOF data described above in comparison with those in literature show that upon the deletion of PsbJ in PsbA1-PSII, the PSII composition may slightly vary from prep to prep. If present, the 3 proteins Psb27, Psb28 and Tsl0063 are in a so minor proportion of the ΔPsbJ-43H/PSII studied here that this proportion will not contribute significantly to the results described thereafter. We cannot eliminate the possibility that these 3 proteins are removed during the PSII purification. This, however, does not modify the fact that the studied ΔPsbJ-43H/PSII does not bind Psb27, Psb28 and Tsl0063.

In *Synechocystis* 6803, the deletion of PsbJ has been proposed to alter both the forward electron flow from Q_A^- to the plastoquinone pool and the back reaction between Q_A^- and the oxidized Mn_4CaO_5 cluster (Regel et al. 2001). These conclusions were done in part from thermoluminescence experiments (Rutherford et al. 1982) in whole cells. Here, similar measurements have been done but in purified WT*1-PSII and ΔPsbJ-43H/PSII. Figure 3 shows the TL curves after 1 flash given at -10°C in WT*1-PSII, black traces, and ΔPsbJ-43H/PSII, red traces. In Panel A, the TL measurements were done without any addition whereas in Panel B they were done in the presence of DCMU. The TL curves in WT*1-PSII arising from the $S_2Q_B^-$ charge recombination in Panel A with a peak temperature at ~43°C and from the $S_2Q_A^-$/DCMU charge recombination in Panel B with a peak temperature at ~13°C are those expected in *T. elongatus* with an heating rate of 0.4°C/s. In ΔPsbJ-43H/PSII, no signal was detected both in Panels A and B. The very small signal around 0°C in Panels A and B is very similar in the absence and the presence of DCMU and therefore cannot arise from the $S_2Q_B^-$ and $S_2Q_A^-$/DCMU charges recombinations studied here. The TL results in Figure 3 differ significantly from those in *Synechocystis* whole cells where in the ΔPsbJ mutant a small TL signal was detected at a slightly lower temperature for the $S_2Q_B^-$ charge recombination and at a slightly higher temperature for the $S_2Q_A^-$/DCMU charge

recombination (Regel et al. 2001). However, the amplitude of a TL signal depends on the proportion of centers with Q_B^- in the dark-adapted state, something that is difficult to control in whole cells. The lack of a TL signal in ΔPsbJ-43H/PSII both with and without DCMU may be explained if 100% of the centers are in the Q_B^- state upon the dark adaptation. As will be shown later, this is not the case in the ΔPsbJ-43H/PSII studied and so another explanation is needed.

The first simple explanation is that the radiative charge recombination in the ΔPsbJ-43H/PSII occurs either *i*) at a temperature much above a bearable temperature for PSII (*i.e.* >> 60°C) or *ii*) at a temperature much lower than 0°C. In the first case, the *Em* of the Q_A/Q_A^- couple, upon the deletion of PsbJ, would be strongly increased and, in the second case, strongly decreased. The second possibility could be a situation in which the Mn_4CaO_5 cluster in the ΔPsbJ-43H/PSII is inactive or lost because we know that under continuous illumination the activity is significantly decreased (Sugiura et al. 2010b).

Before going further in the interpretation of the TL experiments, we have performed some EPR measurements for clarifying the situation.

Figure 4 shows the EPR spectra recorded at 8.6 K in dark-adapted samples (black spectra) and after a continuous illumination at 198 K (red spectra). The blue spectra are the light-*minus*-dark spectra. At 198 K, the electron transfers from Q_A^- to Q_B and from Q_A^- to Q_B^- are blocked so that only one charge separation may occur (Fufezan et al. 2005). In WT*1-PSII, the black spectrum is very similar to the spectrum recorded in PsbA3-PSII under the same conditions, see (Boussac et al. 2011) for a detailed description of the spectra. The signal between 3600 and 5000 gauss originates from $Fe^{2+}Q_B^-$ (Fufezan et al. 2005; Boussac et al. 2011; Sedoud et al. 2011). After illumination at 198 K for ~ 5-10 s, the S_2 multiline signal was formed together with a signal at g = 1.6 (~ 4100 gauss). The g = 1.6 signal originates from the $Q_A^-Fe^{2+}Q_B^-$ state. The $Q_A^-Fe^{2+}$ signal formed in centers with Q_B oxidized prior to the illumination is difficult to detect in the presence of the multiline signal. A careful examination of the blue spectrum in the g = 6 to g = 8 region indicates that the non-heme iron was oxidized in a very small fraction of the dark-adapted centers and was reduced upon the 198 K illumination (Boussac et al. 2011). The spectrum in the dark-adapted ΔPsbJ-43H/PSII also exhibits a $Fe^{2+}Q_B^-$ signal with a somewhat smaller amplitude (see also Figure 7) than in WT*1-PSII. This observation rules out the hypothesis that the lack of a TL signal is due to centers with 100% Q_B^- in the dark-adapted state. In agreement with the MALDI-TOF data above, and as previously reported (Sugiura et al. 2010b), the EPR also shows that the Cytc_{550}

(PsbV) is missing in the purified PSII as evidenced by the much smaller signals at g ~ 3 and g ~ 2.2 (3000 gauss) corresponding to the g_z and g_y resonances of cytochrome signals, respectively (the g_x feature is difficult to detect under the conditions used for the recording of these spectra). We have nevertheless previously shown that PsbV was detectable in the ΔPsbJ-43H/thylakoids (Sugiura et al. 2010b). Cytb_{559} is detected because it is in the low potential oxidized form in ΔPsbJ-43H/PSII (Sugiura et al. 2010). The detection of a signal at g = 6 (~1100 gauss) indicates that a proportion of Cytb_{559} is also present in an oxidized high spin (S = 5/2) configuration. Importantly, the S_2 multiline signal is detectable upon the 198 K illumination with an amplitude close to 60-70 % of that in WT*1-PSII. Therefore, the total absence of a TL signal in this sample is also not due to an inactive or missing Mn_4CaO_5 cluster. The proportion of ΔPsbJ-43H/PSII in which the Mn_4CaO_5 is able to progress to the S_2 state upon an illumination at 198 K is higher than the O_2 evolution activity found in this PSII that is about 30% (Sugiura et al. 2010b). However, it is well known that the O_2 activity under continuous illumination does not necessarily correlate with the proportion of active centers. For example, upon the substitution of Ca^{2+} for Sr^{2+} the O_2 activity under continuous illumination is decreased by a least of factor of 2 whereas all the centers are fully active (Ishida et al. 2008). In an additional control experiment (not shown) aiming at following the period four oscillation measured at 291 nm and 100 ms after each flash of a series (Lavergne 1991; Ishida et al. 2008) it has been found that in the ΔPsbJ-43H/PSII the miss parameter is close to 20% instead of ~ 8% in the PsbA1-PSII.

The remaining possible explanations for the lack of a TL signal in ΔPsbJ-43H/PSII are either *i*) an inefficient charge separation after one flash illumination in contrast to the continuous illumination at 198 K, and/or *ii*) a too fast, even at -10°C, or too slow charge recombination in the temperature range probed by the TL thus preventing the detection of the signal. These possibilities have been tested in the EPR experiments reported in Figure 5 and Figure 6.

Panel A in Figure 5 shows the magnetic field range in which most of the EPR signals are detectable except $Tyr_D^{\bullet}$. The $Tyr_D^{\bullet}$ signal is shown in Panel B. The black spectra were recorded in dark-adapted PSII and they are, of course, similar to those described in Figure 4. The green spectra have been recorded after one saturating flash given at room temperature (~20-22 °C) followed by an as-fast-as possible freezing of the sample (~2 s) in a dry ice bath at 198 K. Then, the red spectra were recorded after a further continuous illumination at 198 K following the one flash illumination. In WT*1-PSII, the difference in the amplitude of the S_2

multiline between the green and red spectra is mainly due to the proportion of centers in which the $S_0Tyr_D^\bullet$ to $S_1Tyr_D^\bullet$ transition occurs with the one flash illumination. As the $Tyr_D^\bullet$ signal (Panel B) does not vary significantly, this suggests that the proportion of centers in which the S_1Tyr_D to $S_1Tyr_D^\bullet$ transition occurs is negligible (Styring and Rutherford 1987).

In contrast, in ΔPsbJ-43H/PSII, upon the illumination at 198 K, the increase of the S_2 multiline and $Tyr_D^\bullet$ signals was much more pronounced than in WT*1-PSII. This results shows that in dark-adapted ΔPsbJ-43H/PSII there is a proportion of centers in the S_1Tyr_D state and a larger proportion of centers in the $S_0Tyr_D^\bullet$ state than in WT*1-PSII. Since the proportion of centers in the $Q_AFe^{2+}Q_B^-$ state is smaller in the ΔPsbJ-43H/PSII than in WT*1-PSII after the dark adaptation, this ratio is inversed after the one flash illumination. Consequently, the illumination at 198 K is expected to induce a larger $Q_A^-Fe^{2+}Q_B^-$ in ΔPsbJ-43H/PSII than in WT*1-PSII and that is indeed what is observed here. It should be mentioned that, normally, an illumination at 198 K is unable to oxidize Tyr_D in active centers. The increase seen in Panel B therefore likely occurs in the proportion of inactive ΔPsbJ-43H/PSII. The important result in this experiment is that the one-flash illumination is able to induce the S_2 state in the ΔPsbJ-43H/PSII although to a slightly less extent than in WT*1-PSII due to a higher proportion of centers in the S_1Tyr_D and $S_0Tyr_D^\bullet$ states and also to a higher miss parameter. The stability of the S_2 state has then been monitored in an experiment corresponding to the TL experiment in the presence of DCMU.

In Figure 6, the black spectra were recorded in dark-adapted PSII without any addition and the red spectra after the addition of DCMU. Two observations can be made here. Firstly, in both WT*1-PSII and ΔPsbJ-43H/PSII, the addition of DCMU resulted in the formation of $Q_A^-Fe^{2+}$/DCMU to the detriment of $Fe^{2+}Q_B^-$ (Velthuys 1981). In both samples, $Q_A^-Fe^{2+}$/DCMU exhibited either the g = 1.9 signal or the g = 1.82 signal (Rutherford et al. 1983, Rutherford and Zimmermann 1984), see below for a better description of the signals in Figure 6. Secondly, in WT*1-PSII, the addition of DCMU also modified the non-heme iron signal as previously observed (Diner and Petrouleas 1987). The blue spectra were then recorded after a continuous illumination at 198 K. The S_2 multiline signal was formed in the open centers, *i.e.* in those with no Q_B^- prior to the addition of DCMU. The larger $Q_A^-Fe^{2+}$ signal at g = 1.9 in ΔPsbJ-43H/PSII than in WT*1-PSII have two possible explanations: *i*) a lower amount of Q_B^- before the addition of DCMU and *ii*) a smaller proportion of oxidized non-heme iron. Indeed, the oxidation of Q_A^- by the oxidized non-heme iron results in the disappearance of the non-

heme iron signal is WT*1-PSII. Unfortunately, in ΔPsbJ-43H/PSII, the presence of the high spin Cytb_{559} signal does not allow the detection of the non-heme iron signal.

After the illumination at 198 K, the samples were immersed for 1 to 2 seconds, in total darkness, in an ethanol bath at 0°C and immediately refrozen in a dry ice bath at 198 K and the green spectra were recorded. In WT*1-PSII, the brief passage at 0°C induced almost no change in the amplitude of the S_2 multiline signal. In contrast, in ΔPsbJ-43H/PSII, almost all the S_2 multiline signal and the g = 1.9 quinone signal disappeared thus showing that the recombination in the $S_2Q_A^-$/DCMU state is very fast at 0°C in this sample. This very likely explains the lack of a TL signal in Figure 3B. The proportion of the g = 1.9 signal which decayed during the warming at 0°C appears larger than the proportion the g = 1.82 signal which decayed. This suggests that the recombination was more efficient with the quinone in the g = 1.9 state than in the g = 1.82 state (Demeter al. 1993; Rutherford, personal communication). Finally, the samples were immersed, in the dark, in an ethanol bath at 20°C and immediately refrozen in a dry ice bath at 198 K and the spectra in magenta were recorded. In WT*1-PSII, the S_2 multiline now decreased significantly as expected from the peak temperature observed in this sample. In ΔPsbJ-43H/PSII, the spectrum was not significantly different from that one after the thawing at 0°C. The recording of the $Tyr_D^\bullet$ spectra as in Panel B of Figure 5 showed again that $Tyr_D^\bullet$ could be induced at 198 K and that a decay occurs upon the short incubation at 0°C (not shown). The experiments described above focused on the charge recombinations. In the following, we will address the forward electron transfer.

Figure 7 shows the flash-induced ΔI/I and its decay at 320 nm after the 2nd flash given on dark-adapted WT*3-PSII (blue), WT*1-PSII (black) and ΔPsbJ-43H/PSII (red). The Q_A^--*minus*-Q_A and Q_B^--*minus*-Q_B difference spectra are similar and have their maximum amplitude at around 320 nm (Schatz and van Gorkom 1985). After the 1st flash and the 3rd flash, the S_1 to S_2 and S_3 to S_0 transitions also contribute significantly to the flash induced absorption changes at 320 nm (Lavergne 1991). In addition, the first flash is also complicated by the Q_A^- to Fe^{2+} electron transfer (Boussac et al. 2011) with possible contribution in this spectral range of the Fe^{3+}/Fe^{2+} couple (Sellés and Boussac, unpublished) and with the formation of the $Tyr_Z^\bullet$ radical in inactive centers (with a flash spacing of 300 ms, the dead centers contribute mainly on the first flash due to the slow decay of $Tyr_Z^\bullet$). For all these reasons, Figure 7 only shows the data after the second flash which is the easiest kinetics to analyze. In centers with Q_B oxidized in the dark-adapted state the flash illumination forms the $Q_A^-Q_B$ state and then the $Q_AQ_B^-$ state. In these centers, the flash-induced ΔI/I does not decay

and it is responsible for the remaining stable ΔI/I at the longest times. In dark-adapted centers with Q_B^- present, the flash illumination forms the $Q_A^-Q_B^-$ state and then the $Q_AQ_BH_2$ state. This reaction is at the origin of the decay in Figure 7 and these kinetics are similar in the 3 samples with a $t_{1/2}$ of 2-3 ms. The similar apparent lag phase with a duration of ~ 1 ms likely corresponds to the electron transfer between Q_A^- and either Q_B or Q_B^-. This experiment shows that the forward electron transfer is not affected by the deletion of PsbJ.

Finally, Figure 8 shows EPR spectra in WT*1-PSII (black spectra) and ΔPsbJ-43H/PSII (red spectra) recorded with a magnetic field scale allowing a better observation of the quinone signals. Panel A shows the $Fe^{2+}Q_B^-$ signal recorded in the dark-adapted samples. The signal is smaller in the ΔPsbJ-43H/PSII as mentioned previously and very slightly shifted. Panel B shows the spectra after a further illumination at 4.2 K. In centers with Q_B^- present in the dark this 4.2 K illumination resulted in the formation of the $Q_A^-Fe^{2+}Q_B^-$ signal that is larger in the WT*1-PSII. In the ΔPsbJ-43H/PSII, consequently to the larger proportion of centers with Q_B in the dark-adapted state, the 4.2 K illumination resulted in a larger proportion of $Q_A^-Fe^{2+}Q_B$ giving rise to the g = 1.9 signal between 3500 and 3700 gauss. Panel C shows the spectra recorded after an illumination at 4.2 K of samples in which a low amount of ferricyanide has been added (less than 100 µM) upon the dark adaptation to have the highest proportion of Q_B without the risk to oxidize the non-heme iron. Although there was still a low amount of $Q_A^-Fe^{2+}Q_B^-$ signal in ΔPsbJ-43H/PSII, in both samples such a procedure resulted in the formation of a similar $Q_A^-Fe^{2+}Q_B$ characterized by the g = 1.9 signal. Finally, in Panel D the spectra were recorded after the addition of DCMU which resulted in the formation of $Q_A^-Fe^{2+}$/DCMU in centers with Q_B^- present in the dark. Two signals are observed in the two samples, the signal at g = 1.9 and a much broader ~ 300 gauss-width signal reminiscent of a signal previously observed (Sedoud et al. 2011). The larger amplitude of these two signals in WT*1-PSII resulted of the higher concentration of Q_B^- in the dark in this PSII.

Discussion

In PSII lacking the PsbJ subunit it is possible to observe a proportion of the enzyme associated to polypeptides known to be assembly cofactors such as Psb27, Psb28 and Tsl0063, and which are not detected in the mature PSII, *e.g.* (Nowaczyk et al. 2006; Roose and Pakrasi 2008; Komenda et al. 2012; Liu et al. 2013; Huang et al. 2021; Zabret et al.

2021). The cryo-EM structure of an intermediate state was resolved (Zabret et al. 2021) with the interesting observation that the bicarbonate ligand of non-heme iron is replaced with a glutamate (glu241 of PsbD), a structural motif found in purple bacteria. Such a motif was further proposed to protect PSII from damage during biogenesis. Although the 3 proteins Psb27, Psb28 and Tsl0063 are possibility detected in the ΔPsbJ-43H/PSII studied here, the MALDI-TOF signals are so weak that we can reasonably consider that the purified PSII studied here is devoid of these assembly cofactors, see also (Sugiura et al. 2010b). The main peptides which are missing in this ΔPsbJ-43H/PSII are PsbY, PsbU and PsbV. Although PsbV is present in the ΔPsbJ-thylakoids (Sugiura et al. 2010b), the g_z value is lower than in intact PSII. This indicates (Roncel et al. 2003) that PsbV is not properly bound to PSII in thylakoids in the absence of PsbJ. Therefore, PsbJ very likely stabilizes the binding of the extrinsic peptides PsbU and PsbV and possibly of the trans-membrane α-helix PsbY as previously suggested (Zabret et al. 2021; Huang et al. 2021; Xiao et al. 2021). The ΔPsbJ-43H/PSII is essentially monomeric (Sugiura et al. 2010b) and in agreement with such a destabilization for PsbY, it was observed that although present, no electron density corresponding to PsbY was found in a crystal of monomeric PSII (Broser et al. 2010).

Despite the close proximity of PsbJ with the Q_B binding pocket, from the data in Figure 8, the lack of this subunit does not dramatically perturb, from an EPR point of view, any of the four states $Q_AFe^{2+}Q_B^-$, $Q_A^-Fe^{2+}Q_B$, $Q_A^-Fe^{2+}Q_B^-$ and $Q_A^-Fe^{2+}$/DCMU. The quinone Q_B is present and DCMU binds in the Q_B pocket, with the same consequences, as in the wild type PSII. Nevertheless, despite the lack of strong structural changes, the energetics is strongly modified. Since a great proportion of ΔPsbJ-43H/PSII has an intact Mn_4CaO_5 cluster, this allowed us to probe these changes by using thermoluminescence (Rutherford 1982; Johnson et al. 1995; Cser and Vass 2007; Rappaport and Lavergne 2009).

In WT*1-PSII, the TL peak corresponding to the $S_2Q_A^-$/DCMU recombination is downshifted by ~32°C, from 45°C to 13°C, when compared to the $S_2Q_B^-$ recombination. According to a correspondence of 0.3-0.4°C/mV estimated by Rappaport and Lavergne (2009), see also (Cser and Vass 2007), this locates the energy level of the $S_2Q_A^-$/DCMU state at least 80 mV (= 32/0.4) above the energy level of the $S_2Q_B^-$ state in WT*1-PSII. If we assume that the *Em* of the Q_A/Q_A^- couple is increased by about 50 mV with DCMU bound as in plant PSII (Krieger et al. 1995), this would locate the energy level of the $S_2Q_A^-$ state at least 80 + 50 = 130 mV above that of the $S_2Q_B^-$ state in WT*1-PSII.

In ΔPsbJ-43H/PSII neither the $S_2Q_A^-$/DCMU nor the $S_2Q_B^-$ charge recombinations are detectable in the temperature range from -10°C to 70°C. The same reasoning done above for the WT*1-PSII would locate the energy level of the $S_2Q_A^-$/DCMU state at least 200 mV (= 80/0.4) above the $S_2Q_B^-$ state in ΔPsbJ-43H/PSII, 80°C being the lower limit for the difference in the TL peaks corresponding to the $S_2Q_A^-$/DCMU and $S_2Q_B^-$ charge recombinations in this sample.

We cannot totally discard the possibility that the release of PsbV affects the stability of S_2 in the ΔPsbJ-43H/PSII. However, *Synechocystis* mutants lacking PsbV exhibit TL peaks at a slightly higher temperature than in the wild type (Shen et al. 1998) suggesting an increase of the S_2 stability that is the opposite of what is seen here.

For analyzing the TL data, two extreme cases will be considered assuming that the effect of the deletion occurs mainly on the acceptor side. In the first one, the deletion of PsbJ would only affect the *Em* of the Q_A/Q_A^- couple whereas in the second case, only the *Em* of the Q_B/Q_B^- couple would be affected. We cannot discard a possible effect on both Q_A and Q_B. In this case, the changes will apply on Q_A and Q_B but to a less extent on each of them.

In the first case, we will assume that in ΔPsbJ-43H/PSII the binding of DCMU also increases the *Em* of the Q_A/Q_A^- couple by ~50 mV as supposed above for WT*1/PSII. Therefore, with an energy level of the $S_2Q_A^-$/DCMU state at least 200 mV above that of the $S_2Q_B^-$ state this would locate the energy level of the $S_2Q_A^-$ state (without DCMU) at least 200+50=250 mV above the $S_2Q_B^-$ state in ΔPsbJ-43H/PSII instead of 130 mV in WT*1-PSII. Although the value of 250 mV could be overestimated, this high value explains the lack of the $S_2Q_B^-$ charge recombination experimentally observed in the TL experiment and the very fast $S_2Q_A^-$/DCMU charge recombination. The decrease in the *Em* of the Q_A/Q_A^- couple could also explain the faster charge recombination observed in *Synechocystis* 6803 (Regel et al. 2001) in the absence of PsbJ if we are in conditions with a large proportion of the quinone pool fully reduced as often observed with whole cells.

In the second case, the *Em* of the Q_B/Q_B^- couple would reach a value disfavoring the electron coming back on Q_A. However, the energy level of the $S_2Q_A^-$/DCMU also needs to be much higher in ΔPsbJ-43H/PSII than in WT*1-PSII to explain the lack of a TL signal in the presence of DCMU above -10°C. Since the peak in WT*1-PSII is observed at 13°C, a peak at a temperature below -10°C correspond to a decrease by at least ~ -58 mV (–23/0.4) for the *Em* of the Q_A/Q_A^- couple in the presence of DCMU when compared to WT*1-PSII. Since PsbJ is close to the Q_B pocket and therefore close to the DCMU binding site, a DCMU effect on the

Em of the Q_A/Q_A^- couple different in ΔPsbJ-43H/PSII than in plant PSII would not be unlikely. If we further push the reasoning assuming no change in the *Em* Q_A/Q_A^- couple in the ΔPsbJ-43H/PSII, the effect of the DCMU binding could be negligible. Indeed, the *Em* of the Q_A/Q_A^- couple with DCMU bound in the ΔPsbJ-43H/PSII would be the same than for the Q_A/Q_A^- couple in the absence of DCMU in WT*1/PSII. A higher *Em* of the Q_B/Q_B^- couple may also explain the lower O_2 evolution under continuous illumination by the ΔPsbJ-43H/PSII (Sugiura et al. 2010b) by decreasing the efficiency of the electron transfer between Q_B^- and the added quinone.

Alone, a low *Em* of the Q_A/Q_A^- couple in ΔPsbJ-43H/PSII is expected to increase the damages due to the repopulation of triplet states in the functional enzyme. For that reason we would favor the model in which only the *Em* of the Q_B/Q_B^- couple is affected (increased) in ΔPsbJ-43H/PSII. The increase of the Δ*Em* between Q_A/Q_A^- and Q_B/Q_B^-, and without affecting the forward electron transfer, could contribute in a protection against the charge recombinations between the donor side and Q_B^-. Such a charge recombination was identified as the origin of the damage by about 2 orders of magnitude higher than induced by the same amount of energy delivered by continuous light (Keren et al. 1997) and a protection against it would favor the photoactivation process, see (Bao and Burnap 2016) for a recent review on photoactivation.

Legends of the figures

Figure 1: Light-induced difference spectra around 545 nm. The flash-induced absorption changes were measured in PsbA1/PSII (black spectrum), ΔPsbJ-43H/PSII (red spectrum) and PsbA3-PSII (blue spectrum). The data points are the average of the ΔI/I values detected 15 µs after the 2nd to 7th actinic flashes given to dark-adapted PSII. After dark adaptation for 1 h at room temperature, 100 µM PPBQ (dissolved in dimethyl sulfoxide) was added to the samples. The amplitude of the spectra were normalized to a Chl concentration corresponding to OD_{673nm}=1.75.

Figure 2: MALDI-TOF MS profiling of PSII subunits. (A) Linear mode MALDI-TOF spectra of subunits from ΔPsbJ-43H/PSII (upper panel) and WT*1-PSII (lower panel) strains. For presentation, both spectra were internally recalibrated on known peaks of PSII subunits using their theoretical average masses (formylated PsbT, *m/z* = 3902.67 Da; PsbK, *m/z* = 4099.88 Da; PsbL, *m/z* = 4297.02 Da; acetylated PsbF, *m/z* = 4975.66 Da; formylated PsbZ, *m/z* = 6792.18 Da; PsbE, *m/z* = 9441.53Da) according to (Sugiura et al. 2010a 2010b, Boussac et al. 2013, Nowaczyk et al. 2012). In the inset, zoom of the 3090-4025 *m/z* range of high-resolution MALDI-TOF spectra from ΔPsbJ-43H/PSII mutant (upper panel) and WT*1-PSII wild-type (lower panel) strains acquired in reflection mode. Both spectra were internally recalibrated on known mono-isotopic peaks of PSII subunits using their theoretical mono-isotopic masses (formylated PsbT, *m/z* = 3900.09 Da; PsbK, *m/z* = 4097.32 Da; PsbL, *m/z* = 4294.32 Da; acetylated PsbF, *m/z* = 4972.61 Da. (B) Linear mode MALDI-TOF spectra of ΔPsbJ-43H/PSII mutant (upper panel) and WT*1/PSII (lower panel) strains. In the upper panel which shows the 11000-15000 *m/z* range for the ΔPsbJ-43H/PSII mutant spectrum, the amplitude was magnified 10 times. (*) this 206 Da mass shift could correspond to farnesyl adduct find in mono-charged and discharged PsbV. There is no peak at 16472 *m/z* which suggests that the peak at 8236 *m/z* does not correspond to a double charged ion. Instead, it could correspond to a contamination by the subunit c of the ATP synthase (Suhai et al. 2008).

Figure 3: Thermoluminescence curves after one flash given at -10°C either without any addition (Panel A) or in the presence of DCMU (Panel B). Black curve, WT*1/PSII; red curve, ΔPsbJ-43H/PSII. The concentration of the samples was adjusted exactly to OD_{673nm}=0.7 (~10 µg Chl/mL) before to be dark-adapted at room temperature for at least 1 h.

In Panel B, the final concentration of DCMU, dissolved in ethanol, was 100 µM. After the addition of DCMU, the samples were immediately loaded into the cuvette in total darkness. The heating rate was 0.4°C/s.

Figure 4: EPR spectra recorded in WT*1-PSII and ΔPsbJ-43H/PSII. The spectra were recorded after dark-adaptation for 1 hour at room temperature (black spectra) and after a continuous illumination at 198 K (red spectra). The blue spectra are the light-*minus*-dark spectra. The concentration was 1.1 mg Chl/mL. Instrument settings: temperature, 8.6 K; modulation amplitude, 25 G; microwave power, 20 mW; microwave frequency, 9.4 GHz; modulation frequency, 100 kHz.

Figure 5: EPR spectra recorded in WT*1/PSII and ΔPsbJ-43H/PSII. The spectra were recorded after dark-adaptation for 1 hour at room temperature (black spectra), after illumination by one flash at room temperature (green spectra) and after a further continuous illumination at 198 K (red spectra). The concentration was 1.1 mg Chl/mL. Instrument settings: temperature, 8.6 K; microwave frequency, 9.4 GHz; modulation frequency, 100 kHz. Modulation amplitude, 25 G and microwave power, 20 mW in Panel A and modulation amplitude, 2.8 G and microwave power, 2 µW in Panel B. In the conditions used for the recording of the $Tyr_D^{\bullet}$ spectra, the microwave power is still slightly saturating so that an increase in the relaxation properties upon the formation of S_2 induces an increase of the signal amplitude (Styring and Rutherford 1988). This effect is larger in the negative part of the signal and is less when using a smaller modulation frequency (not shown) which is indicative of a rapid-passage effect (Styring and Rutherford 1988).

Figure 6: EPR spectra recorded in WT*1-PSII (Panel A) and ΔPsbJ-43H/PSII (Panel B). The spectra were recorded after dark-adaptation for 1 hour at room temperature (black spectra) and after the addition (100 µM) dissolved in ethanol (red spectra). Then, the blue spectra were recorded after an illumination at 198 K. The green spectra were recorded after a brief (1-2 s) warming of the samples at 0°C and the spectra in magenta were recorded after a second brief warming at 20°C. The concentration was 1.1 mg Chl/mL. Instrument settings: temperature, 8.6 K; microwave frequency, 9.4 GHz; modulation frequency, 100 kHz; modulation amplitude, 25 G; microwave power, 20 mW.

Figure 7: Time-courses of the ΔI/I changes at 320 nm after the 2nd flash given on dark-adapted WT*1-PSII (black points), ΔPsbJ-43H/PSII (red points) and WT*3-PSII (blue data points). Flashes spaced 300 ms apart. Chl concentration adjusted to OD_{673nm}=1.75.

Figure 8: EPR spectra recorded in WT*1-PSII (black spectra) and ΔPsbJ-43H/PSII (red spectra). Panel A, the spectra were recorded after dark-adaptation for 1 hour at room temperature. Panel B, the spectra were recorded after a further illumination at 4.2 K. Panel C, the spectra were recorded after the addition of 100 µM of ferricyanide on dark-adapted samples followed by an illumination at 4.2 K. Panel D, the spectra were recorded after the addition of DCMU (100 µM) dissolved in ethanol to dark-adapted samples. The concentration was 1.1 mg Chl/mL. Instrument settings: temperature, 4.2 K except for Panel A in which T = 8.6 K; microwave frequency, 9.4 GHz; modulation frequency, 100 kHz; modulation amplitude, 25 G; microwave power, 20 mW.

References

Bao H, Burnap RL (2016) Photoactivation: The light-driven assembly of the water oxidation complex of Photosystem II. Front Plant Sci 7:article 578. https://doi.org/10.3389/fpls.2016.00578

Beal D, Rappaport F, Joliot P (1999) A new high-sensitivity 10-ns time-resolution spectrophotometric technique adapted to in vivo analysis of the photosynthetic apparatus. Rev Sci Instrum 70: 202–207. https://doi.org/10.1063/1.1149566

Boussac A, Sugiura M, Rappaport F (2011) Probing the quinone binding site of photosystem II from *Thermosynechococcus elongatus* containing either PsbA1 or PsbA3 as the D1 protein through the binding characteristics of herbicides. Biochim Biophys Acta 1807:119–129. https://doi.org/10.1016/j.bbabio.2010.10.004

Broser M, Gabdulkhakov A, Kern J, Guskov A, Muh F, Saenger W, Zouni A (2010) Crystal structure of monomeric Photosystem II from *Thermosynechococcus elongatus* at 3.6-A˚ resolution. J Biol Chem 285: 26255–26262. https://doi.org/10.1074/jbc.M110.127589.

Choo P, Forsman JA, Hui LL, Khaing EP, Summerfield TC, Eaton-Rye JJ (2021) The PsbJ protein is required for photosystem II activity in centers lacking the PsbO and PsbV lumenal subunits. Photosynth Res, early access. https://doi.org/10.1007/s11120-021-00862-y

Cox N, Pantazis DA, Lubitz W (2020) Current understanding of the mechanism of water oxidation in Photosystem II and its relation to XFEL data. Annu. Rev. Biochem. 89:795–820. https://doi.org/10.1146/annurev-biochem-011520-104801

Cser K, Vass I (2007) Radiative and non-radiative charge recombination pathways in Photosystem II studied by thermoluminescence and chlorophyll fluorescence in the cyanobacterium Synechocystis 6803. Biochim Biophys Acta 1767: 233–243. https://doi.org/10.1016/j.bbabio.2007.01.022

Cuni A, Xiong L, Sayre R, Rappaport F, Lavergne J (2004) Modification of the pheophytin midpoint potential in Photosystem II: modulation of the quantum yield of charge separation and of charge recombination pathways. Phys Chem Chem Phys 6: 4825–4831 https://doi.org/10.1039/B407511K

de Causmaecker S, Douglass JS, Fantuzzi A, Nitschke W, Rutherford AW (2019) Energetics of the exchangeable quinone, Q_B, in Photosystem II. Proc Natl Acad Sci USA 116: 19458–19463. www.pnas.org/cgi/doi/10.1073/pnas.1910675116

Demeter S, Goussias C, Bern G, Kovács L, Petrouleas V (1993) Participation of the g = 1.9 and g = 1.82 EPR forms of the semiquinone-iron complex, $Q_A^-Fe^{2+}$ of photosystem II in the generation of the Q and C thermoluminescence bands, respectively. FEBS 336: 352–356. https://doi.org/10.1016/0014-5793(93)80836-J

Diner BA, Petrouleas V (1987) Light-induced oxidation of the acceptor-side Fe(ll) of Photosystem II by exogenous quinones acting through the Q_B binding site. II. Blockage by inhibitors and their effects on the FeIII) EPR spectra. Biochim Biophys Acta 893: 138–148. https://doi.org/10.1016/0005-2728(87)90033-8

Ducruet JM (2003) Chlorophyll thermoluminescence of leaf discs: simple instruments and progress in signal interpretation open the way to new ecophysiological indicators. J Exp Bot 54: 2419–2430. https://doi.org/10.1093/jxb/erg268

Ducruet JM, Vass I (2009) Thermoluminescence: experimental. Photosynth Res 201: 195–204. https://doi.org/10.1007/s11120-009-9436-0

Forsman JA, Eaton-Rye JJ (2021) The interaction between PsbT and the DE loop of D1 in Photosystem II stabilizes the quinone-iron electron acceptor complex. Biochemistry 60: 53–63. https://doi.org/10.1021/acs.biochem.0c00668.

Fufezan C, Zhang CX, Krieger-Liszkay A, Rutherford AW (2005) Secondary quinone in photosystem II of *Thermosynechococcus elongatus*: semiquinone-iron EPR signals and temperature dependence of electron transfer. Biochemistry 44: 12780–12789. https://doi.org/10.1021/bi051000k

Funk C (2000) Functional analysis of the PsbX protein by deletion of the corresponding gene in *Synechocystis sp*. PCC 6803. Plant Mol Biol 44: 815–827. https://doi.org/10.1023/A:1026764728846

Garcia-Cerdan JG, Sveshnikov D, Dewez D, Jansson S, Funk C, Schroder WP (2009) Antisense inhibition of the PsbX protein affects PSII integrity in the higher plant *Arabidopsis thaliana*. Plant Cell Physiol 50: 191–202. https://doi.org/10.1093/pcp/pcn188

Holzwarth AR, Müller MG, Reus M, Nowaczyk M, Sander J, Rögner M (2006) Kinetics and mechanism of electron transfer in intact photosystem II and in the isolated reaction center: pheophytin is the primary electron acceptor. Proc Natl Acad Sci USA 103: 6895–6900. https://doi.org/10.1073/pnas.0505371103

Huang G, Xiao Y, Pi X, Zhaoa L, Zhu Q, Wang W, Kuang T, Han G, Sui S-F, Shen J-R (2021) Structural insights into a dimeric Psb27-photosystem II complex from a cyanobacterium *Thermosynechococcus vulcanus*. Proc Natl Acad Sci USA 118: e2018053118. https://doi.org/10.1073/pnas.2018053118

Hughes JL, Cox N, Rutherford AW, Krausz E, Lai T-L, Boussac A, Sugiura M (2010) D1 protein variants in Photosystem II from *Thermosynechococcus elongatus* studied by low temperature optical spectroscopy. Biochim Biophys Acta 1797: 11–19. https://doi.org/10.1016/j.bbabio.2009.07.007

Inoue-Kashino N, Kashino Y, Takahashi Y (2011) Psb30 is a photosystem II reaction center subunit and is required for optimal growth in high light in *Chlamydomonas reinhardtii*. J Photochem Photobiol 104: 220–228. https://doi.org/10.1016/j.jphotobiol.2011.01.024

Ishida N, Sugiura M, Rappaport F, Lai T-L, Rutherford AW, Boussac A (2008) Biosynthetic exchange of bromide for chloride and strontium for calcium in the photosystem II oxygen-evolving enzyme. J Biol Chem 283: 13330–13340. https://doi.org/10.1074/jbc.M710583200

Iwai M, Suzuki T, Kamiyama A, Sakurai I, Dohmae N, Inoue Y, Ikeuchi M (2010) The PsbK subunit is required for the stable assembly and stability of other small subunits in the PSII complex in the thermophilic cyanobacterium *Thermosynechococcus elongatus* BP-1. Plant Cell Physiol 51: 554–560. https://doi.org/10.1093/pcp/pcq020

Johnson GN, Rutherford AW, Krieger A (1995) A change in the midpoint potential of the quinone QA in Photosystem II associated with photoactivation of oxygen evolution. Biochim Biophys Acta 1229: 202–207. https://doi.org/10.1016/0005-2728(95)00003-2

Joliot P, Kok B (1975) Oxygen evolution in photosynthesis, in: Govindjee (Ed.), Bioenergetics of Photosynthesis, Academic Press, New York, pp. 387–412.

Kaminskaya O, Shuvalov VA, Renger G (2007) Evidence for a novel quinone-binding site in the photosystem II (PS II) complex that regulates the redox potential of cytochrome b559. Biochemistry 46: 1091–1105. https://doi.org/10.1134/S1607672907010048

Kashino Y, Lauber WM, Carroll JA, Wang Q, Whitmarsh J, Satoh K, Pakrasi HB (2002) Proteomic analysis of a highly active photosystem II preparation from the cyanobacterium *Synechocystis* sp. PCC 6803 reveals the presence of novel polypeptides. Biochemistry 41: 8004-8012. https://10.1021/bi026012

Kashino Y, Takahashi T, Inoue-Kashino N, Ban A, Ikeda Y, Satoh K, Sugiura M (2007) Ycf12 is a core subunit in the photosystem II complex. Biochim Biophys Acta 1767: 1269–1275. https://doi.org/10.1016/j.bbabio.2007.08.008

Keren N, Berg A, VanKan PJM, Levanon H, Ohad I (1997) Mechanism of photosystem II photoinactivation and D1 protein degradation at low light: The role of back electron flow. Proc Natl Acad Sci USA 94: 1579–1584. https://doi.org/10.1073/pnas.94.4.1579.

Kok B, Forbush B, McGloin M (1970) Cooperation of charges in photosynthetic O_2 evolution–I. A linear four step mechanism. Photochem Photobiol 11: 457–475. https://doi.org/10.1111/j.1751-1097.1970.tb06017.x

Komenda J, Sobotka R, Nixon PJ (2012) Assembling and maintaining the Photosystem II complex in chloroplasts and cyanobacteria. Curr Opin Plant Biol 15: 245-251; https://doi.org/10.1016/j.pbi.2012.01.017

Krieger A, Rutherford AW, Johnson GN (1995) On the determination of redox midpoint potential of the primary quinone electron acceptor, Q_A, in photosystem II. Biochim Biophys Acta 1229:193–201. https://doi.org/10.1016/0005-2728(95)00002-Z

Lavergne J (1991) Improved UV-visible spectra of the S-transitions in the photosynthetic oxygen-evolving system. Biochim Biophys Acta 1060: 175–188. https://doi.org/10.1016/S0005-2728(09)91005-2

Liu HJ, Chen JW, Huang RYC, Weisz D, Gross ML, Pakrasi HB (2013) Mass Spectrometry-based Footprinting Reveals Structural Dynamics of Loop E of the Chlorophyll-binding Protein CP43 during Photosystem II Assembly in the Cyanobacterium *Synechocystis* 6803. J Biol Chem 288: 14212–14220. https://doi.org/10.1074/jbc.M113.467613

Luo H, Jackson SA, Fagerlund RD, Summerfield TC, Eaton-Rye JJ (2014) The importance of the hydrophilic region of PsbL for the plastoquinone electron acceptor complex of Photosystem II. Biochim Biophys Acta 1837: 1435–1446. https://doi.org/10.1016/j.bbabio.2014.02.015

Merry SAP, Nixon PJ, Barter LMC, Schilstra MJ, Porter G, Barber J, Durrant JR, Klug D (1998) Modulation of quantum yield of primary radical pair formation in photosystem II by site directed mutagenesis affecting radical cations and anions. Biochemistry 37: 17439–17447. https://doi.org/10.1021/bi980502d

Müh F, Zouni A (2005) Extinction coefficients and critical solubilisation concentrations of photosystems I and II from *Thermosynechococcus elongatus*. Biochim Biophys Acta 1708: 219–228. https://doi.org/10.1016/j.bbabio.2005.03.005

Müh F, Glöckner C, Hellmich J, Zouni A (2012) Light-induced quinone reduction in photosystem II. Biochim Biophys Acta 1817: 44–65. https://doi.org/10.1016/j.bbabio.2011.05.021

Mulo P, Sicora C, Aro E-M (2009) Cyanobacterial psbA gene family: optimization of oxygenic photosynthesis. Cell Mol Life Sci 66: 3697–3710. https://doi.org/10.1007/s00018-009-0103-6

Nowaczyk MM, Hebeler R, Schlodder E, Meyer HE, Warscheid B, Rogner M (2006) Psb27, a cyanobacterial lipoprotein, is involved in the repair cycle of photosystem II. Plant Cell 18: 3121–3131. https://doi.org/10.1105/tpc.106.042671

Nowaczyk MM, Krause K, Mieseler M, Sczibilanski A, Ikeuchi M, Rögner M (2012) Deletion of psbJ leads to accumulation of Psb27–Psb28 photosystem II complexes in *Thermosynechococcus elongatus*. Biochim Biophys Acta 1817: 1339–1345. http://dx.doi.org/10.1016/j.bbabio.2012.02.017

Ohad I, Dal Bosco C, Herrmann RG, Meurer J (2004) Photosystem II proteins PsbL and PsbJ regulate electron flow to the plastoquinone pool. Biochemistry 43: 2297–2308. https://doi.org/10.1021/bi0348260

Rappaport F, Lavergne J (2009) Thermoluminescence: theory. Photosynth Res 101:205–216. https://doi.org/10.1007/s11120-009-9437-z

Regel RE, Ivleva NB, Zer H, Meurer J, Shestakov SV, Herrmann RG, Pakrasi HB, Ohad I (2001) Deregulation of electron flow within Photosystem II in the absence of the PsbJ protein. J Biol Chem 276: 41473–41478. https://doi.org/10.1074/jbc.M102007200

Romero E, Novoderezhkin VI, van Grondelle R (2017) Quantum design of photosynthesis for bio-inspired solar-energy conversion. Nature 543: 355–365. https://doi.org/10.1038/nature22012

Roncel M, Boussac A, Zurita JL, Bottin H, Sugiura M, Kirilovsky D, Ortega J-M (2003) Redox properties of the photosystem II cytochromes b559 and c550 in the cyanobacterium *Thermosynechococcus elongatus*. J Biol Inorg Chem 8: 206–216. https://doi.org/10.1007/s00775-002-0406-7

Roose JL, Pakrasi HB (2008) The Psb27 protein facilitates manganese cluster assembly in photosystem II. J Biol Chem 283:4044–4050. https://doi.org/10.1074/jbc.M708960200

Roose JL, Frankel LK, Mummadisetti MP, Bricker TM (2016) The extrinsic proteins of photosystem II: update. Planta 243: 889–908. https://doi.org/10.1007/s00425-015-2462-6

Rutherford AW, Crofts AR, Inoue Y (1982) Thermoluminescence as a probe of Photosystem II photochemistry. The origin of the flash-induced glow peaks. Biochim Biophys Acta 682: 457–465. https://doi.org/10.1016/0005-2728(82)90061-5

Rutherford AW, Zimmermann J-L (1984) A new EPR signal attributed to the primary plastosemiquinone acceptor in Photosystem II. Biochim Biophys Acta 767: 168–175. https://doi.org/10.1016/0005-2728(84)90092-6

Rutherford AW, Zimmermann J-L, Mathis P (1983) The effect of herbicides on components of the PS II reaction centre measured by EPR. Febs lett 165: 156–162. https://doi.org/10.1016/0014-5793(84)80161-1

Rutherford AW, Krieger-Liszkay A (2001) Herbicide-induced oxidative stress in photosystem II. Trends Biochem Sci 26: 648–653. https://doi.org/10.1016/S0968-0004(01)01953-3

Sedoud A, Cox N, Sugiura M, Lubitz W, Boussac A, Rutherford AW (2011) The semiquinone-iron complex of Photosystem II: EPR signals assigned to the low field edge of the ground state doublet of $Q_A^{\bullet}$-Fe^{2+} and $Q_B^{\bullet}$-Fe^{2+}. Biochemistry 50: 6012–6021. https://doi.org/10.1021/bi200313p

Schatz GH, van Gorkom HJ (1985) Absorbance difference spectra upon charge transfer to secondary donors and acceptors in Photosystem II, Biochim Biophys Acta 810: 283–294. https://doi.org/10.1016/0005-2728(85)90212-9

Shen JR (2015) The structure of Photosystem II and the mechanism of water oxidation in photosynthesis. Annu Rev Plant Biol 66: 23–48. https://doi.org/10.1146/annurev-arplant-050312-120129

Shen J-R, Qian M, Inoue Y, Burnap RL (1998) Functional characterization of *Synechocystis* sp. PCC 6803 ΔpsbU and ΔpsbV mutants reveals important roles of cytochrome c-550 in cyanobacterial oxygen evolution. Biochemistry 37: 1551-1558. https://doi.org/10.1021/bi971676i

Sheridan KJ, Duncan EJ, Eaton-Rye JJ, Summerfield TC (2020) The diversity and distribution of D1 proteins in cyanobacteria. Photosynth Res 145: 111–128. https://doi.org/10.1007/s11120-020-00762-7

Shibuya Y, Takahashi R, Okubo T, Suzuki H, Sugiura M, Noguchi T (2010) Hydrogen bond interaction of the pheophytin electron acceptor and its radical anion in Photosystem II as revealed by Fourier Transform Infrared Difference Spectroscopy. Biochemistry 49: 493–501. https://doi.org/10.1021/bi9018829

Styring S, Rutherford AW (1987) In the oxygen-evolving complex of photosystem II the S_0-state is oxidized to the S_1-state by D^+ (signal-II slow). Biochemistry 26: 2401–2405. https://doi.org/10.1021/bi00383a001

Styring S, Rutherford AW (1988) The microwave power saturation of SII_{slow} varies with the redox state of the oxygen-evolving complex in photosystem II. Biochemistry 27: 4915–4923. https://doi.org/10.1021/bi00413a049.

Suga M, Akita F, Hirata K, Ueno G, Murakami H, Nakajima Y, Shimizu T, Yamashita K, Yamamoto M, Ago H, Shen J-R (2015) Native structure of photosystem II at 1.95 angstrom resolution viewed by femtosecond X-ray pulses. Nature 517: 99–103. https://doi.org/10.1038/nature13991

Sugiura M, Rappaport F, Brettel K, Noguchi T, Rutherford AW, Boussac A (2004) Site-directed mutagenesis of *Thermosynechococcus elongatus* photosystem II: the O_2 evolving enzyme lacking the redox active tyrosine D. Biochemistry 43: 13549–13563. https://doi.org/10.1021/bi048732h

Sugiura M, Boussac A (2014) Some Photosystem II properties depending on the D1 protein variants in *Thermosynechococcus elongatus*. Biochim Biophys Acta 1837: 1427–1434. https://doi.org/10.1016/j.bbabio.2013.12.011

Sugiura M, Inoue Y (1999) Highly purified thermo-stable oxygen evolving Photosystem II core complex from the thermophilic cyanobacterium *Synechococcus elongatus* having His-tagged CP43. Plant Cell Physiol 40: 1219–1231. https://doi.org/10.1093/oxfordjournals.pcp.a029510

Sugiura M, Harada S, Manabe T, Hayashi H, Kashino Y, Boussac A (2010a) Psb30 contributes to structurally stabilise the Photosystem II complex in the thermophilic cyanobacterium *Thermosynechococcus elongatus*. Biochim Biophys Acta 1797: 1546–1554. https://doi.org/10.1016/j.bbabio.2010.03.020

Sugiura M, Iwai E, Hayashi H, Boussac A (2010b) Differences in the interactions between the subunits of Photosystem II dependent on D1 protein variants in the thermophilic cyanobacterium *Thermosynechococcus elongatus*. J Biol Chem 285: 30008–30018. https://doi.org/10.1074/jbc.M110.136945

Sugiura M, Azami C, Koyama K, Rutherford AW, Rappaport F, Boussac A (2014) Modification of the pheophytin redox potential in *Thermosynechococcus elongatus* Photosystem II with PsbA3 as D1. Biochim Biophys Acta 1837: 139–148. https://doi.org/10.1016/j.bbabio.2013.09.009

Sugiura M, Taniguchi T, Tango N, Nakamura M, Sellés J, Boussac A (2020) Probing the role of arginine 323 of the D1 protein in photosystem II function. Physiol Plant 171: 183–199. https://doi.org/10.1111/ppl.13115

Suhai T, Dencher NA, Poetsch A, Seelert H (2008) Remarkable stability of the proton translocating F1F0-ATP synthase from the thermophilic cyanobacterium *Thermosynechococcus elongatus* BP-1. Biochim Biophys Acta 1778: 1131-1140. https://doi.org/10.1016/j.bbamem.2007.12.017

Takasaka K, Iwai M, Umena Y, Kawakami K, Ohmori Y, Ikeuchi M, Takahashi Y, Kamiya N, Shen JR (2010) Deletion Structural and functional studies on Ycf12 (Psb30) and PsbZ-deletion mutants from a thermophilic cyanobacterium. Biochim Biophys Acta 1797: 278–284. https://doi.org/10.1016/j.bbabio.2009.11.001

Umena Y, Kawakami K, Shen J-R, Kamiya N (2011) Crystal structure of oxygen-evolving Photosystem II at a resolution of 1.9 angstrom. Nature 473: 55–60. https://doi.org/10.1038/nature09913

Uto S, Kawakami K, Umena Y, Iwai M, Ikeuchi M, Shen JR, Kamiya N (2017) Mutual relationships between structural and functional changes in a PsbM-deletion mutant of photosystem II. Faraday Discuss198: 107–120. https://doi.org/10.1039/C6FD00213G

van Eerden FJ, Melo MN, Frederix PWJM, Periole X, Marrink SJ (2017) Exchange pathways of plastoquinone and plastoquinol in the photosystem II complex. Nature Comm 8:15214. https://doi.org/10.1038/ncomms15214

Velthuys BR (1981) Electron-dependent competition between plastoquinone and inhibitors for binding to Photosystem-II. Feb let 126: 277–281. https://doi.org/10.1016/0014-5793(81)80260-8

Xiao Y, Huang G, You X, Zhu Q, Wang W, Kuang T, Han G, Sui S-F, Shen J-R (2021) Structural insights into cyanobacterial photosystem II intermediates associated with Psb28 and Tsl0063. Nature Plants, 7: 1132–1142. https://doi.org/10.1038/s41477-021-00961-7

Zabret J, Bohn S, Schuller SK, Arnolds O, Möller M, Meier-Credo J, Liauw P, Chan A, Tajkhorshid E, Langer JD, Stoll R, Krieger-Liszkay A, Engel BD, Rudack T, Schuller JM, Nowaczyk MM (2021) Structural insights into photosystem II assembly. Nature Plants 7: 524–538. https://doi.org/10.1038/s41477-021-00895-0

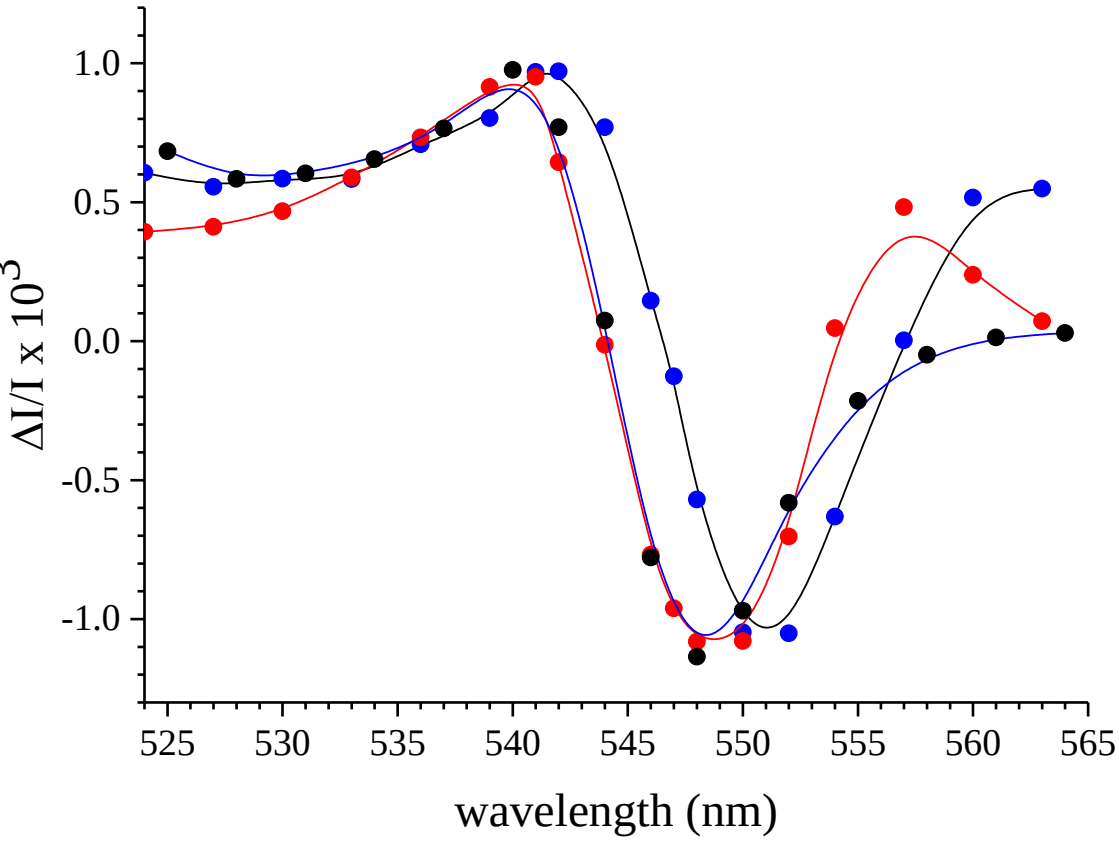

Fig. 1

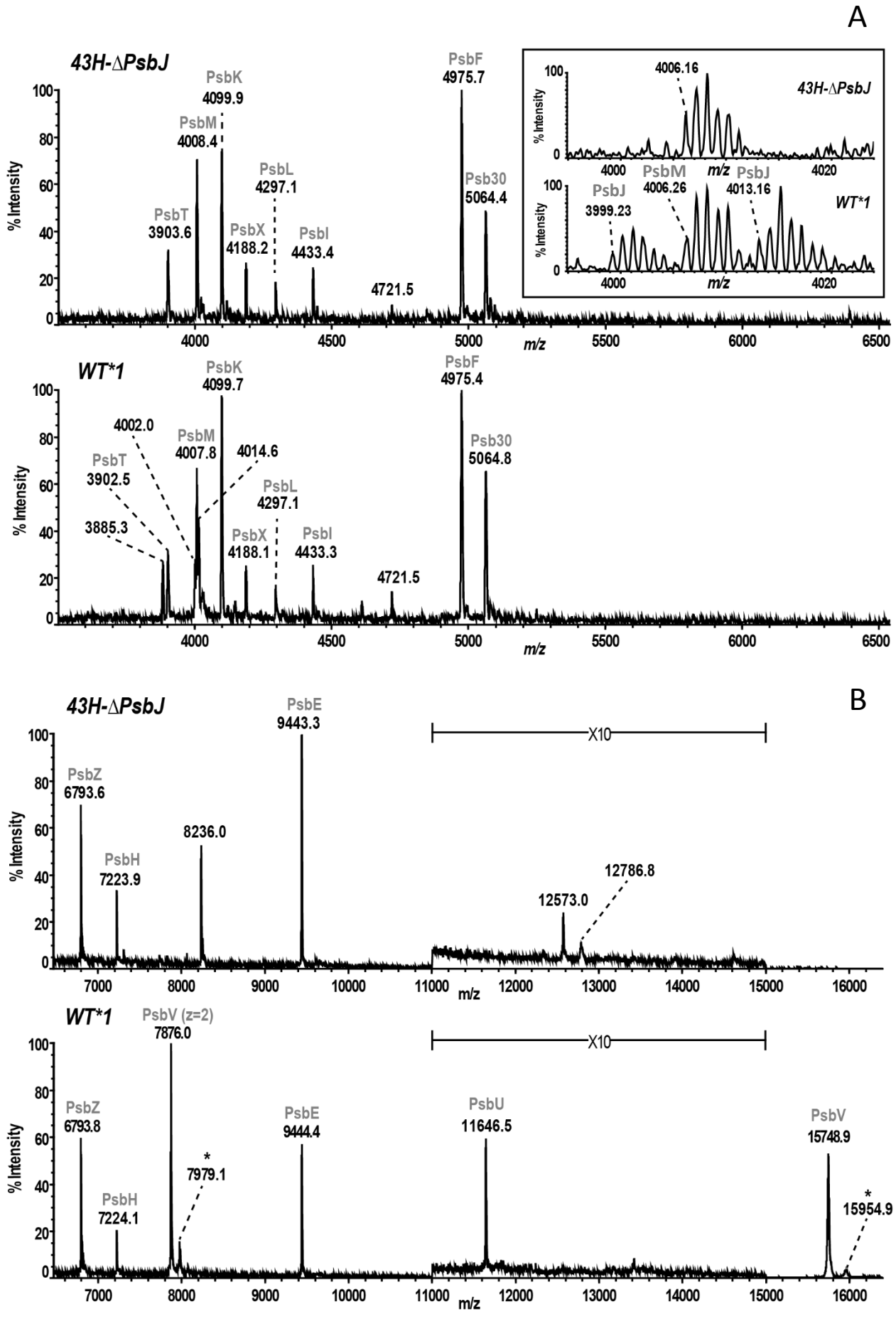
A
43H-ΔPsbJ
PsbK
4099.9
PsbM
4008.4
PsbL
4297.1
PsbT
3903.6
PsbX
4188.2
PsbI
4433.4
4721.5
PsbF
4975.7
Psb30
5064.4
% Intensity
m/z
4006.16
43H-ΔPsbJ
PsbJ
3999.23
PsbM
4006.26
PsbJ
4013.16
WT*1
WT*1
PsbK
4099.7
4002.0
PsbM
4007.8
4014.6
PsbT
3902.5
PsbL
4297.1
3885.3
PsbX
4188.1
PsbI
4433.3
4721.5
PsbF
4975.4
Psb30
5064.8
B
43H-ΔPsbJ
PsbE
9443.3
X10
PsbZ
6793.6
8236.0
PsbH
7223.9
12786.8
12573.0
WT*1
PsbV (z=2)
7876.0
X10
PsbZ
6793.8
PsbE
9444.4
PsbU
11646.5
PsbV
15748.9
*
7979.1
PsbH
7224.1
*
15954.9

Fig. 2

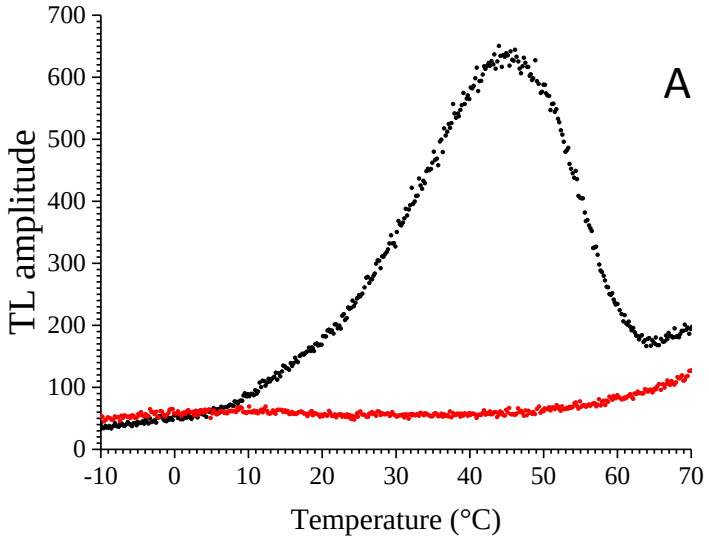
A
TL amplitude
Temperature (°C)
0
100
200
300
400
500
600
700
-10
0
10
20
30
40
50
60
70

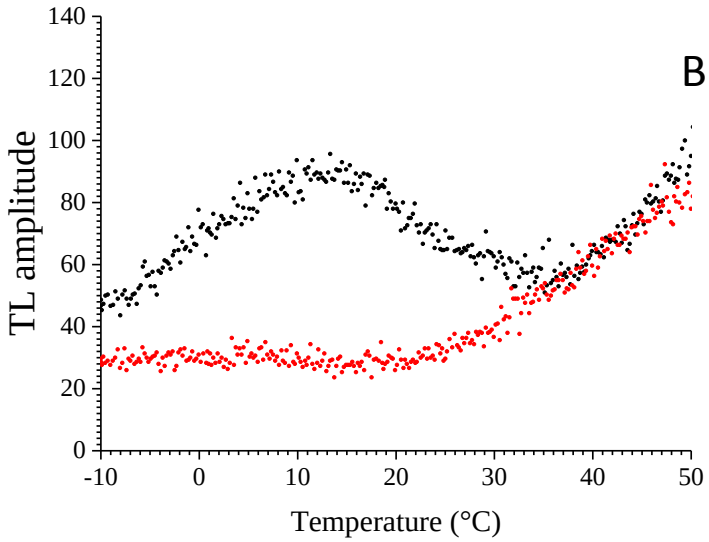
B
TL amplitude
Temperature (°C)
0
20
40
60
80
100
120
140
-10
0
10
20
30
40
50

Fig. 3

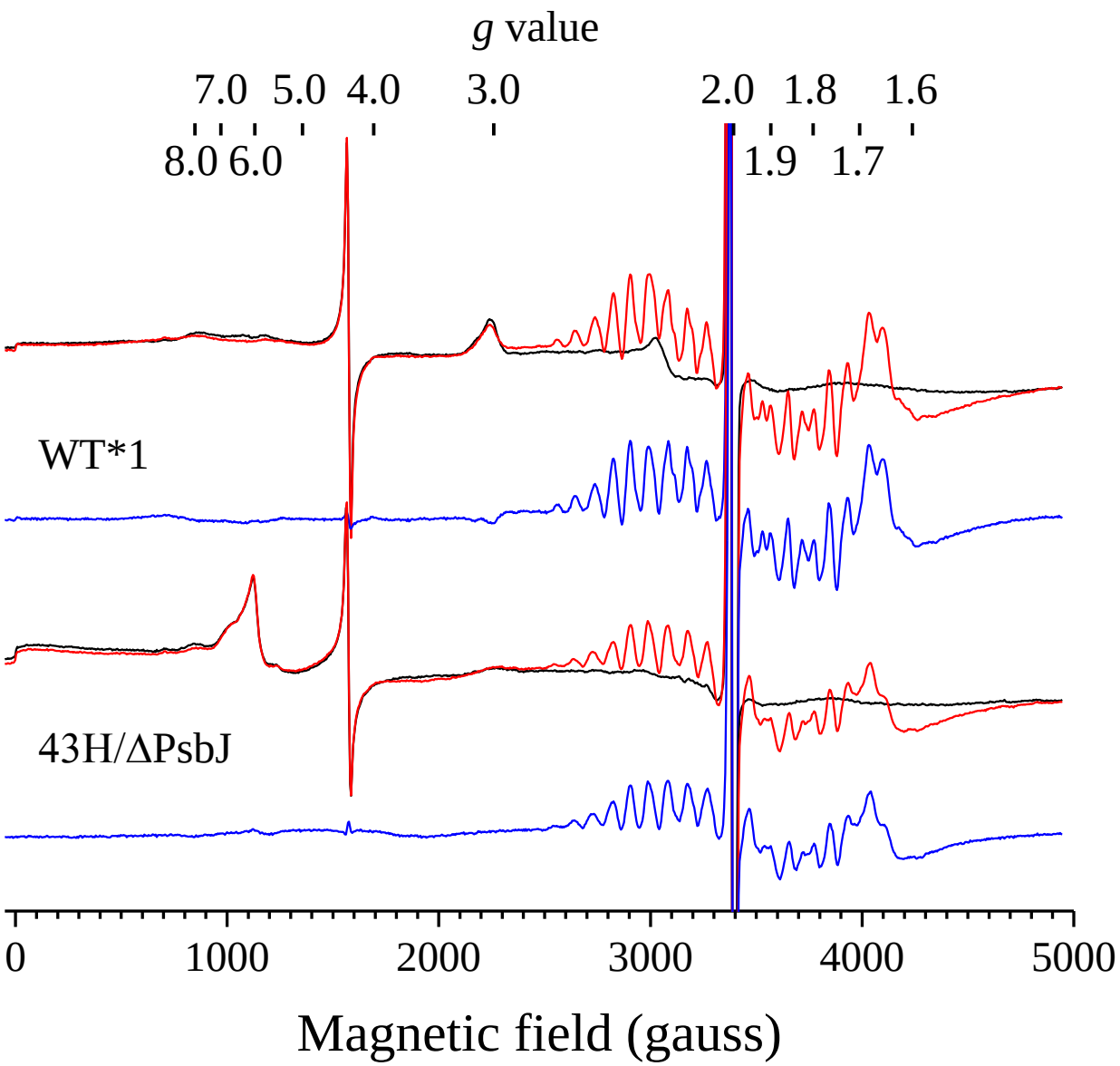
g value
7.0
5.0
4.0
3.0
2.0
1.8
1.6
8.0
6.0
1.9
1.7
WT*1
43H/ΔPsbJ
0
1000
2000
3000
4000
5000
Magnetic field (gauss)

Fig. 4

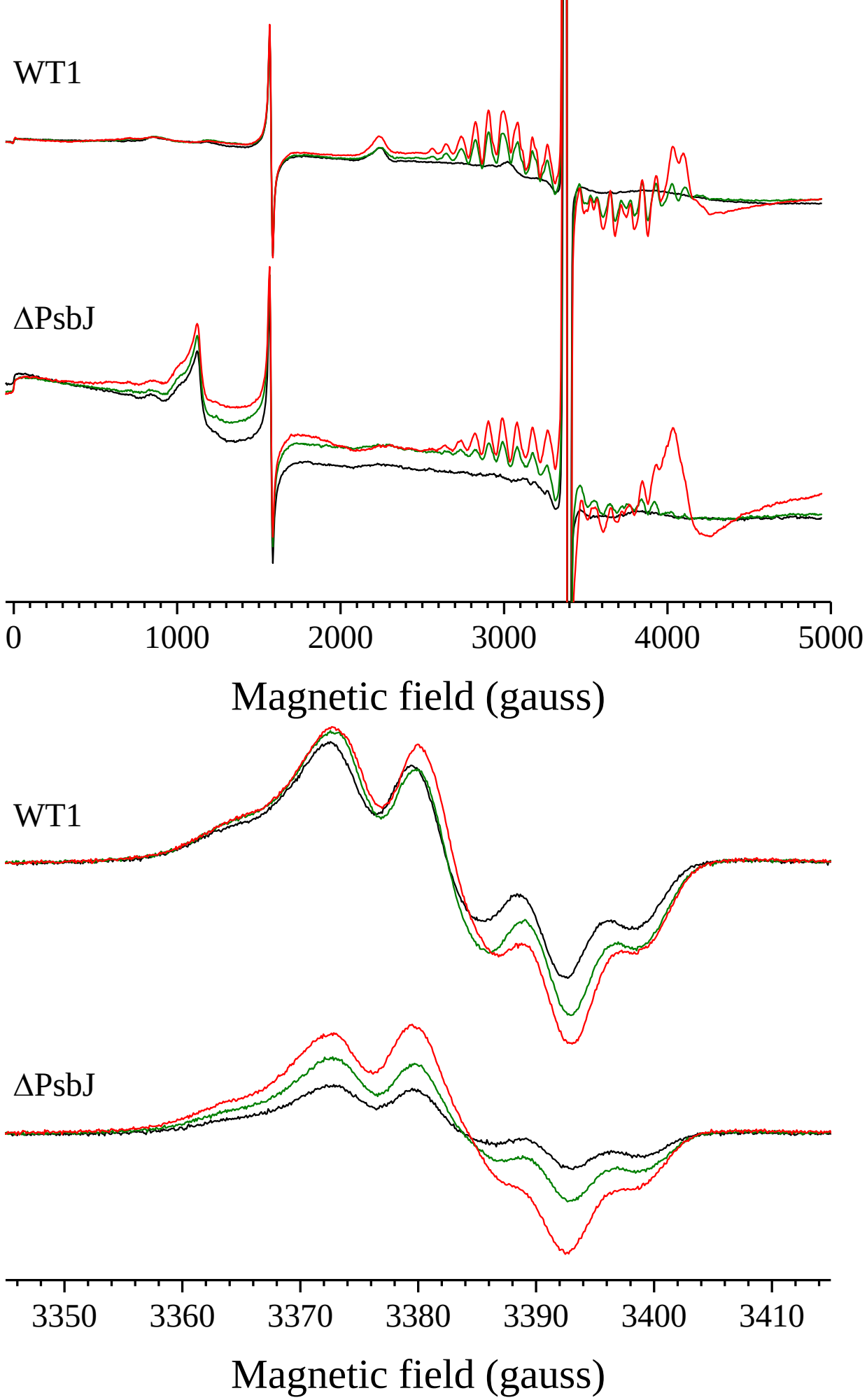
WT1
ΔPsbJ
0
1000
2000
3000
4000
5000
Magnetic field (gauss)
WT1
ΔPsbJ
3350
3360
3370
3380
3390
3400
3410
Magnetic field (gauss)

Fig. 5

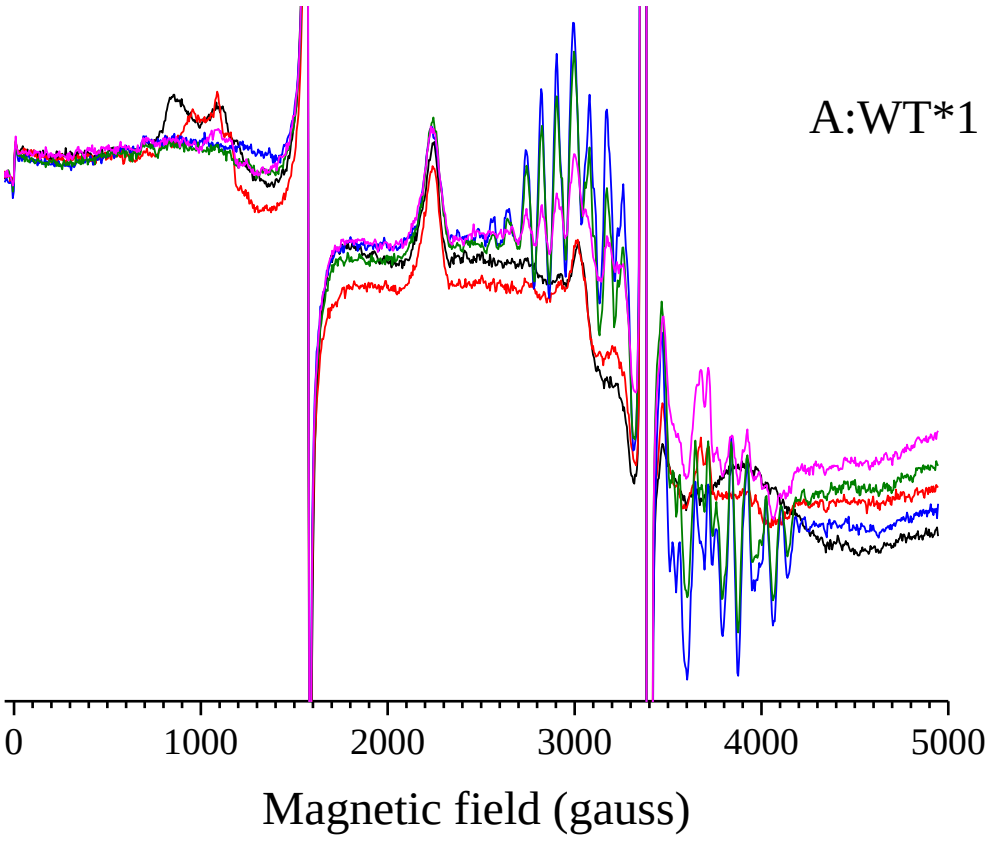
A:WT*1
0
1000
2000
3000
4000
5000
Magnetic field (gauss)

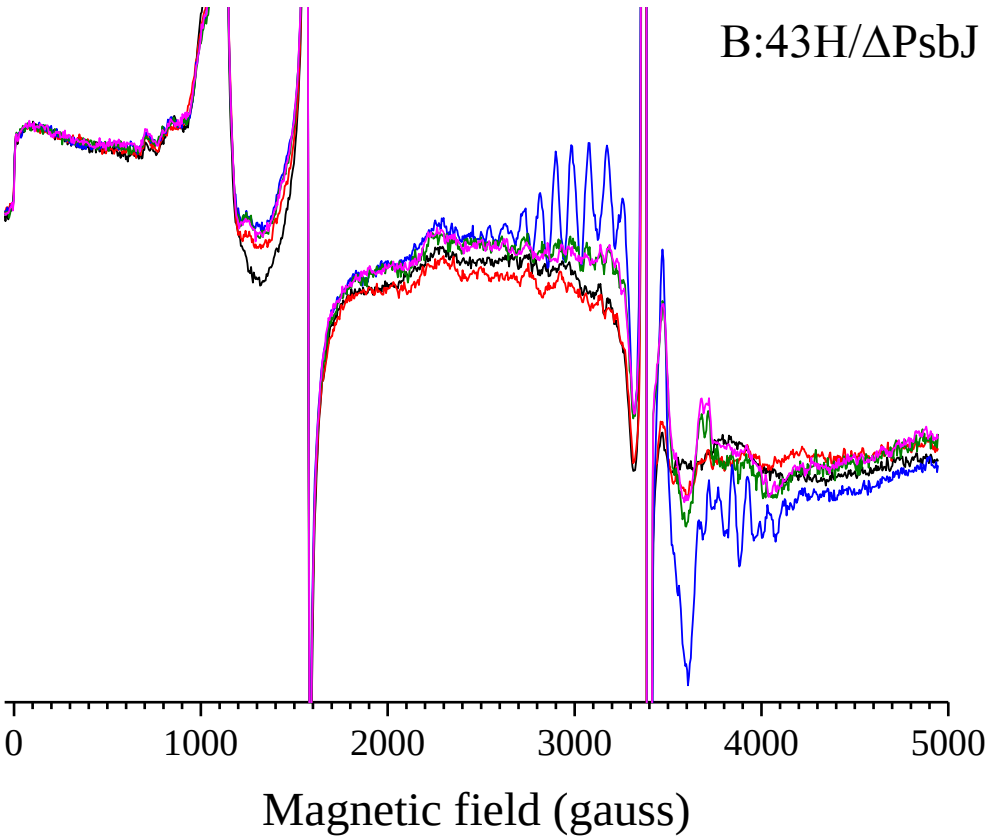
B:43H/ΔPsbJ
0
1000
2000
3000
4000
5000
Magnetic field (gauss)

Fig. 6

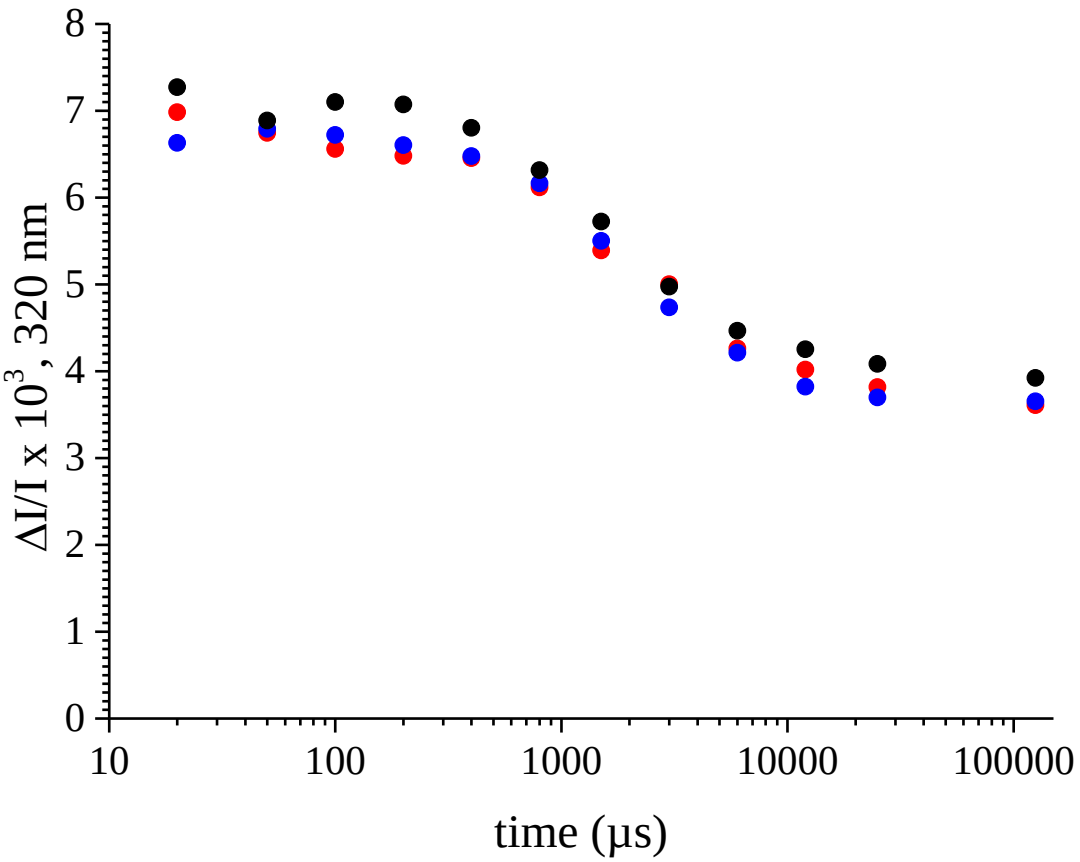

Fig. 7

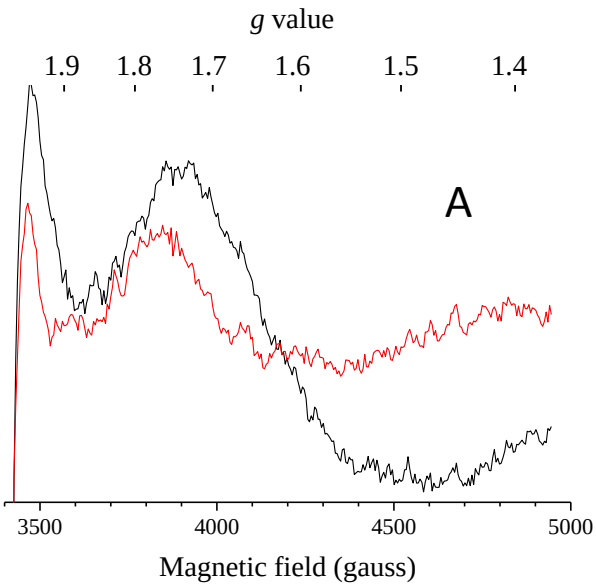
g value
1.9
1.8
1.7
1.6
1.5
1.4
A
3500
4000
4500
5000
Magnetic field (gauss)

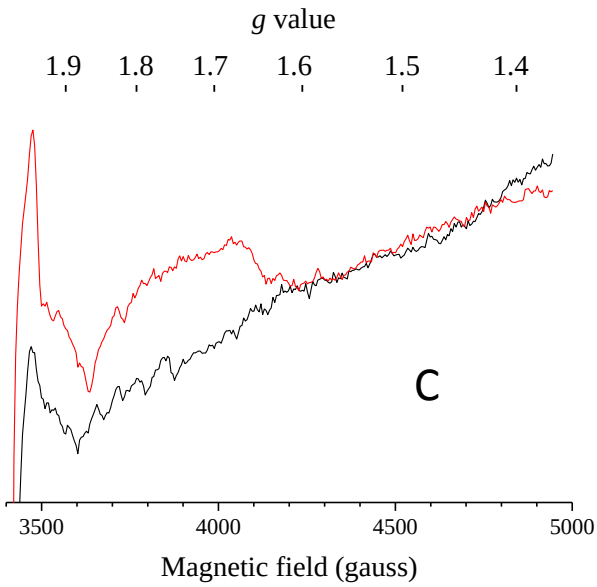
g value
1.9
1.8
1.7
1.6
1.5
1.4
C
3500
4000
4500
5000
Magnetic field (gauss)

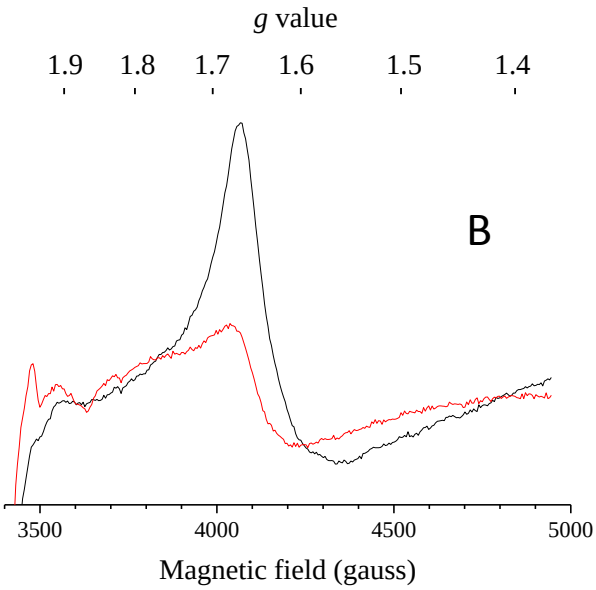
g value
1.9
1.8
1.7
1.6
1.5
1.4
B
3500
4000
4500
5000
Magnetic field (gauss)

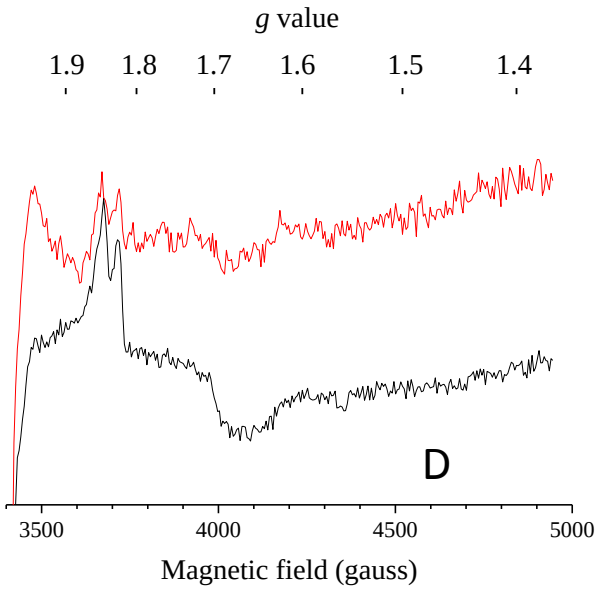
g value
1.9
1.8
1.7
1.6
1.5
1.4
D
3500
4000
4500
5000
Magnetic field (gauss)

Fig. 8